

Operon *flv4-flv2* Provides Cyanobacterial Photosystem II with Flexibility of Electron Transfer

Pengpeng Zhang,^a Marion Eisenhut,^{a,1} Anna-Maria Brandt,^b Dalton Carmel,^a Henna M. Silén,^a Imre Vass,^c Yagut Allahverdiyeva,^a Tiina A. Salminen,^b and Eva-Mari Aro^{a,2}

^aDepartment of Biochemistry and Food Chemistry, Molecular Plant Biology, University of Turku, 20520 Turku, Finland

^bDepartment of Biochemistry and Pharmacy, Structural Bioinformatics Laboratory, Åbo Akademi University, 20520 Turku, Finland

^cInstitute of Plant Biology, Biological Research Center, 6726 Szeged, Hungary

***Synechocystis* sp PCC 6803 has four genes encoding flavodiiron proteins (FDPs; Flv1 to Flv4). Here, we investigated the *flv4-flv2* operon encoding the Flv4, Sll0218, and Flv2 proteins, which are strongly expressed under low inorganic carbon conditions (i.e., air level of CO₂) but become repressed at elevated CO₂ conditions. Different from FDP homodimers in anaerobic microbes, *Synechocystis* Flv2 and Flv4 form a heterodimer. It is located in cytoplasm but also has a high affinity to membrane in the presence of cations. Sll0218, on the contrary, resides in the thylakoid membrane in association with a high molecular mass protein complex. Sll0218 operates partially independently of Flv2/Flv4. It stabilizes the photosystem II (PSII) dimers, and according to biophysical measurements opens up a novel electron transfer pathway to the Flv2/Flv4 heterodimer from PSII. Constructed homology models suggest efficient electron transfer in heterodimeric Flv2/Flv4. It is suggested that Flv2/Flv4 binds to thylakoids in light, mediates electron transfer from PSII, and concomitantly regulates the association of phycobilisomes with PSII. The function of the *flv4-flv2* operon provides many β -cyanobacteria with a so far unknown photoprotection mechanism that evolved in parallel with oxygen-evolving PSII.**

INTRODUCTION

Flavodiiron proteins (FDPs), originally known as A-type flavo-proteins (Flv) (Wasserfallen et al., 1998), function in detoxification of O₂ and/or NO in many strict and facultative anaerobes (Vicente et al., 2008a). FDPs form a complex group of enzymes, and many of them have been thoroughly characterized. Purified FDPs have been shown to function as homodimers or homotetramers (Vicente et al., 2008b, 2009), and many structures have been solved by x-ray crystallography (Frazão et al., 2000; Silaghi-Dumitrescu et al., 2005; Seedorf et al., 2007; Di Matteo et al., 2008). All members of the FDP family share a common minimal core containing two structural domains. The N-terminal metallo- β -lactamase-like domain harbors a nonheme diiron center, and the C-terminal flavodoxin domain contains a flavin mononucleotide (FMN) moiety. The crystal structure has revealed a head-to-tail arrangement of the two FDP monomers, which is required for efficient electron transfer in the active site by bringing the diiron center from one monomer into close contact with the FMN moiety of the other monomer (Vicente et al., 2008a). Despite continuously accumulating

knowledge, the definite answers on substrate specificity of many FDPs have remained unknown.

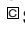
Besides the common sequence core, some of the FDPs have extra C-terminal extensions. Phylogenetic analysis revealed that FDPs bearing the same C-terminal extensions cluster together (Saraiva et al., 2004). All cyanobacterial FDPs examined so far as well as some photosynthetic eukaryotic FDPs contain a C-terminal flavin reductase domain (Zhang et al., 2009). In *Synechocystis* sp PCC 6803 (hereafter *Synechocystis*), four genes encoding FDPs were identified. The *flv1* (*sll1521*) and *flv3* (*sll0550*) genes are dispersed in the genome, whereas *flv2* (*sll0219*) and *flv4* (*sll0217*) are organized in an operon (CyanoBase: <http://genome.kazusa.or.jp/cyanobase/>). Recombinant *Synechocystis* Flv3 homodimer has been shown to have NAD(P)H: oxygen oxidoreductase activity (Vicente et al., 2002). It was soon confirmed by in vivo studies that *Synechocystis* Flv1 and Flv3 function in the Mehler-like reaction, which acquires electrons after photosystem I (PSI) to reduce molecular oxygen to water like the real Mehler reaction but differs from that by no concomitant formation of reactive oxygen species (Helman et al., 2003). We recently showed that up to 60% of electrons from water-splitting photosystem II (PSII) can be directed to molecular oxygen via Flv1 and Flv3 upon inorganic carbon (Ci) starvation in *Synechocystis* 6803 (Allahverdiyeva et al., 2011).

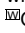
Evolution of oxygenic photosynthesis exposed autotrophic organisms to a special demand of protection against reactive oxygen species to cope with highly oxidizing chemistry of PSII under constant changes in the light supply in natural environments. Several photoprotection mechanisms have evolved in oxygenic photosynthetic organisms, which rapidly modify the existing components to adjust the light-harvesting and energy dissipation functions of the photosynthetic apparatus (Niyogi, 1999; Kanervo et al., 2005; Bailey and Grossman, 2008; Tikkanen

¹ Current address: Plant Biochemistry, Heinrich-Heine-Universitaet Duesseldorf, 40225 Duesseldorf, Germany.

² Address correspondence to evaaro@utu.fi.

The author responsible for distribution of materials integral to the findings presented in this article in accordance with the policy described in the Instructions for Authors (www.plantcell.org) is: Eva-Mari Aro (evaaro@utu.fi).

 Some figures in this article are displayed in color online but in black and white in the print edition.

 Online version contains Web-only data.

www.plantcell.org/cgi/doi/10.1105/tpc.111.094417

et al., 2011). State 1–state 2 transitions (state transitions) (reviewed in Allen, 1992; van Thor et al., 1998; Wollman, 2001; Mullineaux and Emlin-Jones, 2005; Tikkanen et al., 2011) and nonphotochemical quenching (reviewed in Horton et al., 1996; Müller et al., 2001), both based on the light-harvesting antenna systems, are particularly important in short-term regulation of light harvesting in plants and green algae. In cyanobacteria, phycobilisomes (PBSs) function as a major light-harvesting antenna, and their quenching is mediated by a soluble orange carotenoid binding protein, OCP (El Bissati et al., 2000; Kirilovsky, 2007). The Flv2 and Flv4 proteins, unique for cyanobacteria, are also likely to function in photoprotection of PSII (Zhang et al., 2009). Light is an elusive substrate for all photoautotrophs, and photodamage to PSII occurs at all irradiance levels (Tyystjärvi and Aro, 1996). Cyanobacteria are particularly sensitive to light at low ambient CO₂ levels (i.e., air level) when the electron acceptors are limiting photosynthesis. Noteworthy, these are the conditions that also strongly enhance the expression of the *flv4-flv2* operon (Zhang et al., 2009).

The functional mechanisms of the *flv4-flv2* operon (*slI0217-19*), encoding the Flv4, SlI0218, and Flv2 proteins, in apparent photoprotection of PSII have so far remained completely unknown. Here, we propose a unique mechanism for the Flv2, Flv4, and SlI0218 proteins in modulation of PSII function upon stress conditions.

RESULTS

Occurrence of the Operon *flv4-flv2* in Cyanobacteria

Cyanobacterial genomes harbor several copies of FDP genes that occur in pairs and cluster with their genetically close orthologs (Zhang et al., 2009). In *Synechocystis*, the *flv4*, *slI0218*, and *flv2* genes form an operon that belongs to the low Ci stimulon (M. Eisenhut, J. Georg, S. Klähn, I. Sakurai, H. Silén, P. Zhang, W.R. Hess, and E.-M. Aro, unpublished data). Analysis of the sequenced cyanobacterial genomes revealed that the order of the genes in the operon is highly conserved (Figure 1). In this respect, only two exceptions were observed. One is *Nostoc punctiforme* ATCC 29,133 lacking the *flv4* ortholog, which most probably results from the upstream transposase gene (Figure 1). The other exception is *Thermosynechococcus elongatus* BP-1, whose *flv4* (*tlr1088*) and *flv2* (*tll1373*) genes are scattered in the genome, and the *slI0218* ortholog is absent.

SlI0218 is annotated as a hypothetical protein that belongs to the PsiE (for phosphate starvation inducible E) superfamily (<http://www.ncbi.nlm.nih.gov/cdd>) and whose function remains to be determined. SlI0218 orthologs, besides those located in the *flv4-flv2* operons, can be found in many sequenced cyanobacteria, bacteria, and archaea. Phylogenetic analysis (see Supplemental Figure 1 online) grouped the SlI0218 homologs into three clades. Those encoded by the *flv4-flv2* operon are highly conserved and constitute one clade. Other bacteria and archaea sequences grouped into another clade. Interestingly, some filamentous cyanobacteria have two to three copies of SlI0218 homologs. SlI0218 homologs outside the *flv4-flv2* operon in filamentous cyanobacteria form the third clade and are more related to those in bacteria and archaea. It is worth noting that the *flv4-flv2* operon

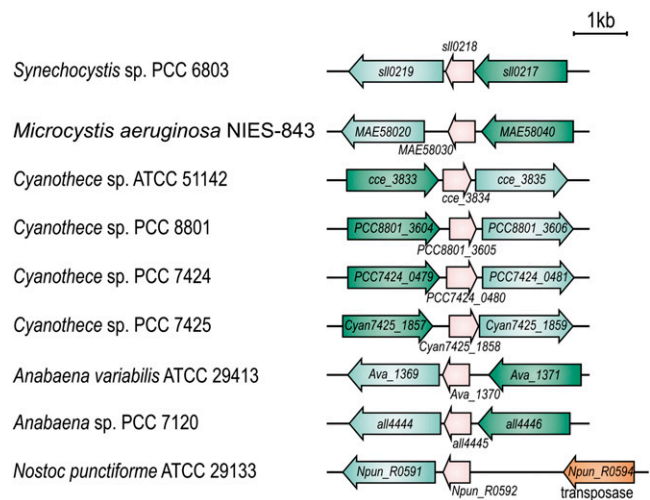


Figure 1. Organization of the *flv4-flv2* Operon in *Synechocystis* sp PCC 6803 and Other Cyanobacterial Species.

Genes are shown in scale. The direction of transcription is indicated by block arrows. The gene numbers/names are given according to CyanoBase. Orthologs are shown by the same color: *flv4* in green, *slI0218* in pink, and *flv2* in cyan.

was not identified in *Synechococcus* species and *Lyngbya*, yet the high homology SlI0218 sequences were found, which grouped together with SlI0218 in the operon clade.

Cellular Location of the Gene Products of the *flv4-flv2* Operon

The transmembrane helix prediction program TMHMM (<http://www.cbs.dtu.dk/services/TMHMM/>) provided evidence that SlI0218 is mainly composed of four transmembrane helices and, therefore, most probably resides in the membrane. Although no transmembrane helices were predicted in any of the FDP sequences, we also found a strong association of the Flv2 and Flv4 proteins with the membrane fraction (Zhang et al., 2009). To localize the Flv4, SlI0218, and Flv2 proteins precisely in the membrane fraction, the thylakoid and plasma membranes, purified by the two-phase partitioning method (Norling et al., 1998), were probed with protein specific antibodies. Unexpectedly, only a weak response was detected with Flv4 and Flv2 antibodies compared with that recorded in the total membrane fraction isolated by a standard method used in our laboratory (which includes high cation concentration; see Methods). However, no SlI0218 signal could be found in conventional two-phase fractions (Norling et al., 1998; Figure 2A).

Nearly complete absence of the Flv4, SlI0218, and Flv2 proteins in the thylakoid and plasma membrane fractions purified by the conventional two-phase partitioning system (Norling et al., 1998) (Figure 2A) needed clarification. To this end, the Flv4, SlI0218, and Flv2 proteins were first analyzed from the total membrane (thylakoids plus plasma membrane) and soluble fractions of the wild-type cells. The fractions were isolated by two different buffer systems, buffer A and buffer B. Buffer A is a low ionic buffer used for the two-phase partitioning (Norling

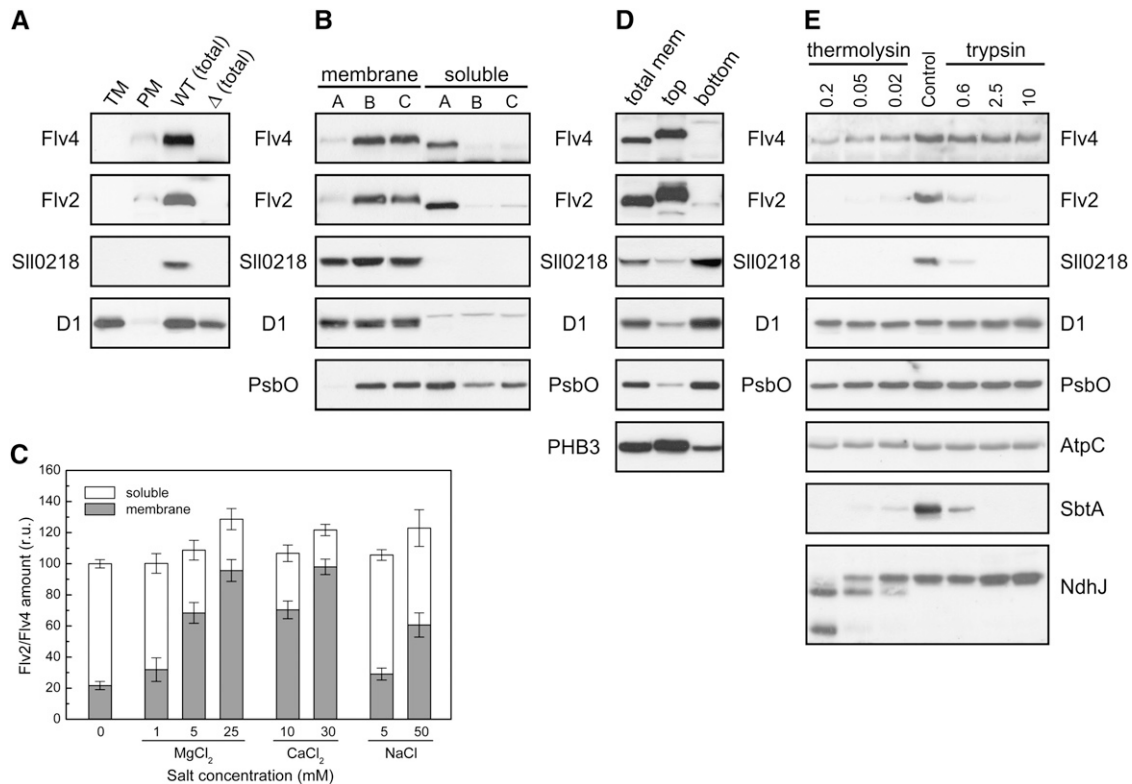


Figure 2. Cellular Locations of the Flv4 (SII0217), SII0218, and Flv2 (SII0219) Proteins in *Synechocystis*.

(A) Thylakoid membrane (TM) and plasma membrane (PM) were purified from wild-type total membranes according to Norling et al. (1998), and total membranes from the wild type (WT [total]) and Δ sII0217-18 mutant (Δ [total]) were isolated as described in Methods.

(B) Comparison of the distribution of the Flv2, SII0218, and Flv4 proteins in the membrane and soluble fractions isolated by different buffer systems: buffer A (no Mg^{2+} or Ca^{2+}), buffer B (30 mM $CaCl_2$), and buffer C (25 mM $MgCl_2$ was supplemented in buffer A).

(C) Relative distribution of the Flv2 and Flv4 proteins in the membrane and soluble fractions upon breaking the wild-type cells in the isolation buffer supplemented with different concentration of $MgCl_2$, $CaCl_2$, and NaCl. The amount of proteins was shown in relative units (r.u.), and the amount obtained by the buffer with no cation was set as 100. Flv2 and Flv4 proteins showed similar partitioning, which is highly dependent on the concentration of Mg^{2+} and Ca^{2+} ions.

(D) Distribution of the Flv4, SII0218, and Flv2 proteins in the membrane fraction. Total membranes (mem) were isolated using buffer D (25 mM $MgCl_2$) and further fractionated by a modified two-phase partitioning system as described in Methods.

(E) Stability of the Flv4, SII0218, and Flv2 proteins in the membrane subjected to proteolysis by different concentration of trypsin (μ g/mL) or thermolysin (mg/mL).

The cells were grown at air level of CO_2 . The Flv4, SII0218, and Flv2 proteins were detected by protein immunoblot. D1 and PsbO of PSII were marker proteins of the thylakoid membrane and the lumen, respectively, and prohibitin 3 (PHB3) was used as a marker protein of the plasma membrane.

et al., 1998), whereas buffer B is a high ionic buffer generally used for PSII isolation (30 mM $CaCl_2$). As shown in Figure 2B, the two buffer systems gave completely different results. The Flv4 and Flv2 proteins were largely released to the soluble fraction with buffer A but remained associated with the membrane with buffer B. When buffer A was supplemented with 25 mM $MgCl_2$, the Flv4 and Flv2 proteins were mainly associated with the membrane fraction, similar to buffer B system. Indeed, the Flv4 and Flv2 proteins could be localized either in the membrane or the soluble fraction, the distribution being largely dependent on the concentration of cation, Ca^{2+} or Mg^{2+} , in the isolation buffer (Figure 2C). Upon increasing the Mg^{2+} or Ca^{2+} concentration, the majority of the Flv2 and Flv4 proteins altered their location from the soluble fraction to the membrane (Figure

2C). On the contrary, the SII0218 protein was detected only in the membrane fraction, independently of the buffer system.

To address the association of the Flv4, Flv2, and SII0218 proteins with the thylakoid or the plasma membrane, membrane isolation was performed in HEPES at pH 7.5 by addition of 25 mM $MgCl_2$, and the pH of the two-phase partitioning buffers was lowered from pH 7.8 to 7.4. As shown in Figure 2D, Flv4 and Flv2 were enriched in the top phase, whereas SII0218 was enriched in the bottom phase. According to immunoblot analysis with several marker proteins, the plasma membrane was shown to be enriched in the top phase and the thylakoid membrane in the bottom phase, thus revealing the association of Flv4 and Flv2 at high cation concentration with the plasma membrane but being soluble at low cation concentration. SII0218 was associated with

the thylakoid membrane independently of the cation concentration (Figure 2B).

The question why SII0218 could be detected neither in the thylakoid nor in the plasma membrane after fractionation in the original two-phase partitioning buffer system (Figure 2A) still remained unanswered. Recent proteomics study of *Synechocystis* thylakoid membrane fraction also failed to identify the SII0218 protein (Pisareva et al., 2011). Such data suggest heterogeneity in the distribution of SII0218 in the thylakoid membrane. To test this hypothesis, the total *Synechocystis* membrane fraction isolated in buffer B, which contains the thylakoid membrane mainly in right-side-out orientation (Figure 2B), was subjected to protease treatment using both trypsin and thermolysin. Intactness of the thylakoid during trypsin digestion was first evidenced by no loss of the PsbO protein, a lumenal extrinsic PSII subunit (Figure 2E). Digestion with thermolysin, on the contrary, decreased the amount of PsbO, suggesting leakage of the thylakoid membrane. Intactness upon trypsin digestion of the NdhJ subunit of NDH-1 on the cytoplasmic side of the thylakoid membrane indicated that this side of the thylakoid membrane was well sealed against trypsin. However, increasing concentration of thermolysin resulted in complete digestion of NdhJ, indicating that the enzyme had penetrated through the thylakoids and opened the membrane sealing completely. Interestingly, the SII0218 protein was easily digested by both trypsin and thermolysin, opposite to the other integral membrane proteins like D1 of PSII and AtpC. This is in apparent contradiction with data in Figure 2B indicating that trypsin cannot access either the cytoplasmic or the lumenal side of the well-sealed thylakoid membrane during the treatment. Direct access of SII0218 to proteolysis by both enzymes indicated that the distribution of the SII0218 protein cannot be homogeneous throughout the thylakoid membrane in the cell. Rather, the SII0218 protein is likely to be located in specific well-exposed regions of the thylakoid membrane. Such thylakoid regions may be largely lost during two-phase partitioning, which is dependent on membrane surface properties.

Expression of the *flv4-flv2* Operon in Various *flv* Inactivation Mutants

It was next investigated whether the presence of the Flv4, SII0218, and Flv2 proteins in *Synechocystis* cells is independent of the other partner proteins encoded by the *flv4-flv2* operon or whether their stability at protein level relies on cotranscribed partners. To this end, the expression of the *flv4-flv2* operon was investigated in the wild type and mutants with interruption of the operon at different positions (Figure 3). Inactivation of *flv2*, or both the *flv2* and the *sII0218* gene, repressed the expression of the Flv4 protein to <50% of that in the wild type (Figure 3C), despite the fact that the transcripts of the *flv4* gene were up-regulated fivefold compared with the wild type (Figure 3B). On the contrary, inactivation of the *flv2* gene resulted in elevated expression of the *sII0218* gene at both the transcript and the protein level. These data indicated a strong regulation of the Flv4 protein, at least an order of magnitude, by the presence or absence of the Flv2 protein. Such coregulation at protein level seems to be independent of the SII0218 protein. Strong

coregulation of the Flv4 and Flv2 proteins and their colocalization both in the presence or absence of cations (Figure 2) suggested a possibility for Flv2/Flv4 heterodimer formation in the cell.

Protein Complexes Formed by the Flv4, SII0218, and Flv2 Proteins

All studied FDPs in anaerobic microbes have a homodimer or homotetramer structure in vitro, and the dimer formation indeed is a necessity for enzymatic activity (Vicente et al., 2008a). It is conceivable that cyanobacterial Flv2 and Flv4 also form dimers. To verify this assumption, the thylakoids were isolated in buffer B (with 30 mM CaCl₂), and protein complexes were solubilized by *n*-dodecyl- β -*D*-maltoside (DM), separated by blue native (BN)-PAGE, and subjected to protein immunoblotting as described (Zhang et al., 2004). However, the extraction of the Flv4 and Flv2 proteins from the membranes by DM or other nonionic detergents turned extremely inefficient (see Supplemental Figure 2 online). To help the identification of the weak signal obtained from the membrane fraction by the Flv2 antibody, we analyzed the soluble fraction as well. As shown in Figure 4A, the Flv2 protein (molecular mass = 65 kD) formed a complex of ~140 kD, which run in BN gels slightly faster than the SbtA complex, a sodium bicarbonate antiporter involved in carbon concentration (Zhang et al., 2004). The immunosignal obtained with the Flv2 antibody in BN blots was verified by protein immunoblot of the two-dimensional (2D) BN/SDS gel (see Supplemental Figure 3 online).

The size of the Flv2 protein complex in BN-PAGE (Figure 4A) corresponded to that of an Flv dimer. To dissect whether the band represented an Flv2 homodimer or an Flv2/Flv4 heterodimer, the Flv4 protein had to be identified. However, the Flv4 polyclonal antibody was not compatible with BN gels and no specific immunoresponse was detected. To solve this problem, the Flv4 protein was fused with a FLAG-tag, and the FLAG-Flv4 protein was expressed both in the wild type and the Δ *sII0218-19* mutant. Using the antibody against FLAG-tag revealed two specific bands in the BN gel blot of the *flag-flv4* strain, corresponding to a dimer (red arrow) and a monomer (green arrow) (Figure 4B). The specificity of the FLAG-tag immunosignals to FLAG-Flv4 was verified by protein immunoblot analysis of the 2D BN/SDS gel (see Supplemental Figure 3 online). Different from the *flag-flv4* strain, the dimeric FLAG-Flv4 form was nearly missing from the Δ *sII0218-19/flag-flv4* strain (Figure 4B), providing evidence that the FLAG-Flv4 protein did not form dimers in the absence of the Flv2 protein. Thus, the dimeric Flv4 complex in *flag-flv4* was assigned as an Flv2/Flv4 heterodimer. Although a considerable amount of monomeric FLAG-Flv4 was detected in the *flag-flv4* and Δ *sII0218-19/flag-flv4* strains, the Flv2 protein was detected only as a dimeric form in the wild type (Figures 4A and 4B). Two possible reasons can lead to this situation: Increase in Flv4 expression in the FLAG-tag strains causes accumulation of excess FLAG-Flv4 protein for stoichiometric formation of the Flv2/Flv4 heterodimer, or introduction of the FLAG-tag might hamper the dimer formation of Flv4. Enhancement of the accumulation of the Flv4 protein in the *flag-flv4* and Δ *sII0218-19/flag-flv4* strains is shown in Supplemental Figure 4A online.

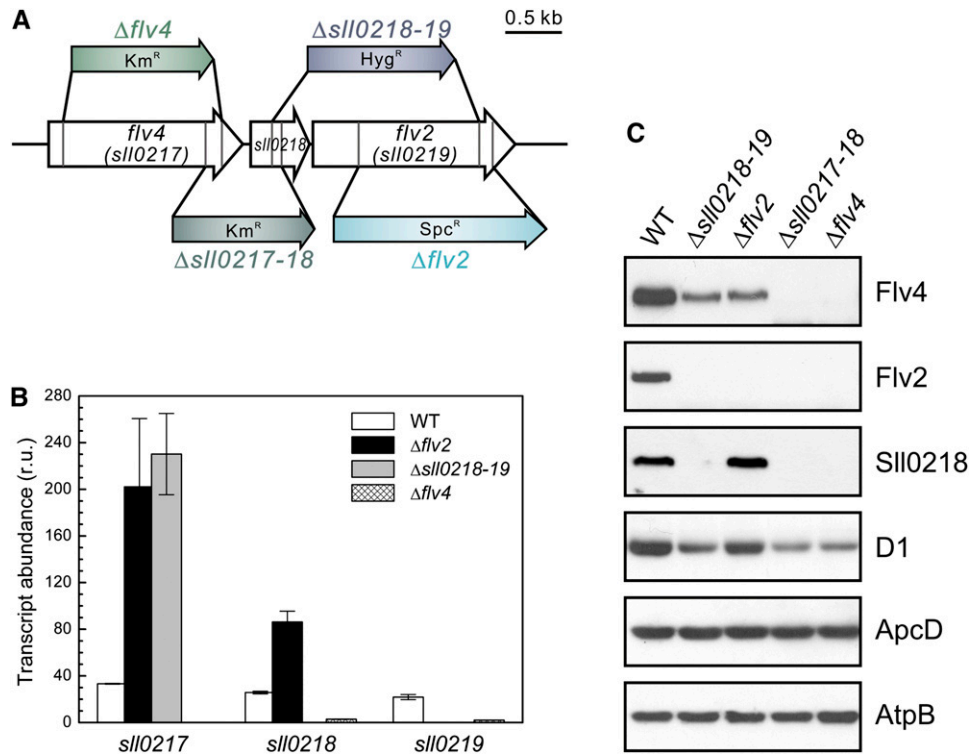


Figure 3. Description of *flv* Inactivation Mutants and the Expression of the Operon *flv4 -flv2* at Air Level of CO_2 .

(A) Schematic description of the four *flv* inactivation mutants mostly used in this study and the location of the kanamycin- (Km), hygromycin- (Hyg), or spectinomycin (Spc)-resistant cassette at different positions.

(B) Transcript accumulation of *sII0217-19* in the wild type (WT) and the three *flv* mutants analyzed by real-time quantitative RT-PCR. Transcription abundance is shown as relative units (r.u.). The transcript level of the *mpb* gene is used as a reference. The results are the mean from three independent experiments \pm SD.

(C) Protein immunoblot demonstrating the protein accumulation of Flv4, SII0218, and Flv2 in the total cell extract from wild type and the four *flv* mutants. [See online article for color version of this figure.]

To investigate the possibility of Flv2 homodimer formation in vivo, the Flv2 protein was expressed under strong *psbA2* promoter in the $\Delta flv4$ and $\Delta sII0218-19$ mutants. The expression pattern of the Flv2 and Flv4 proteins is shown in Supplemental Figure 4B online. Under high CO_2 , where the native *flv4-flv2* promoter is suppressed and, thus, the Flv4 protein is absent, ~60% of the Flv2 proteins were present as homodimers and 40% as monomers, similarly in both complemented strains. When the cells were grown under air level of CO_2 , the pattern of Flv2 in $\Delta flv4::flv2$ was similar to that observed in cells grown under high CO_2 , whereas the amount of monomeric Flv2 largely decreased in the $\Delta sII0218-19::flv2$ strain (i.e., in the presence of the Flv4 protein) (Figure 4B). It is worth noting that the dimeric Flv2 separated by BN-PAGE from the wild type, $\Delta psbA2$, and $\Delta sII0218-19::flv2$ strains grown under air level of CO_2 migrates slightly faster than the Flv2 dimer from high- CO_2 -grown $\Delta flv4::flv2$ and $\Delta sII0218-19::flv2$ cells, also suggesting that the Flv2 dimer complex in the wild type is the Flv2/Flv4 heterodimer (Figure 4B). Interestingly, the accumulation of the Flv2 protein in $\Delta sII0218-19::flv2$ was higher when grown under air level of CO_2 than under high CO_2 (see Supplemental Figure 4B online), which contradicts with the higher expression level of *PpsbA2* under

high CO_2 . This provides further support for coregulation of Flv2 and Flv4 at protein level and, thus, for the formation of the heterodimer in vivo.

Contrary to the apparent heterodimer association of the Flv2 and Flv4 proteins, the SII0218 protein was always found to be associated with a much larger complex, higher than 500 kD in size, which in BN-PAGE was found to be located between the PSII dimer and the NDH-1L complex (Zhang et al., 2004; Figure 4C). The expression of the NDH-1 complex (probed by the NdhJ antibody) in $\Delta sII0218-19$ was similar to that in the wild type, and the SII0218 complex was normal also in the M55 strain (lacking both the NDH-1L and NDH-1M), suggesting that the SII0218 protein is not associated with the NDH-1L complex. Nevertheless, a faint band, overlapping with the α -SII0218 band, was observed with the D2 antibody particularly in the wild-type cells, suggesting a possible association of SII0218 with an intermediate stage of PSII assembly.

PSII Complexes in the *flv* Mutants

To clarify the effects at the level of the PSII complexes, the membranes of the wild type and the various *flv* mutants were

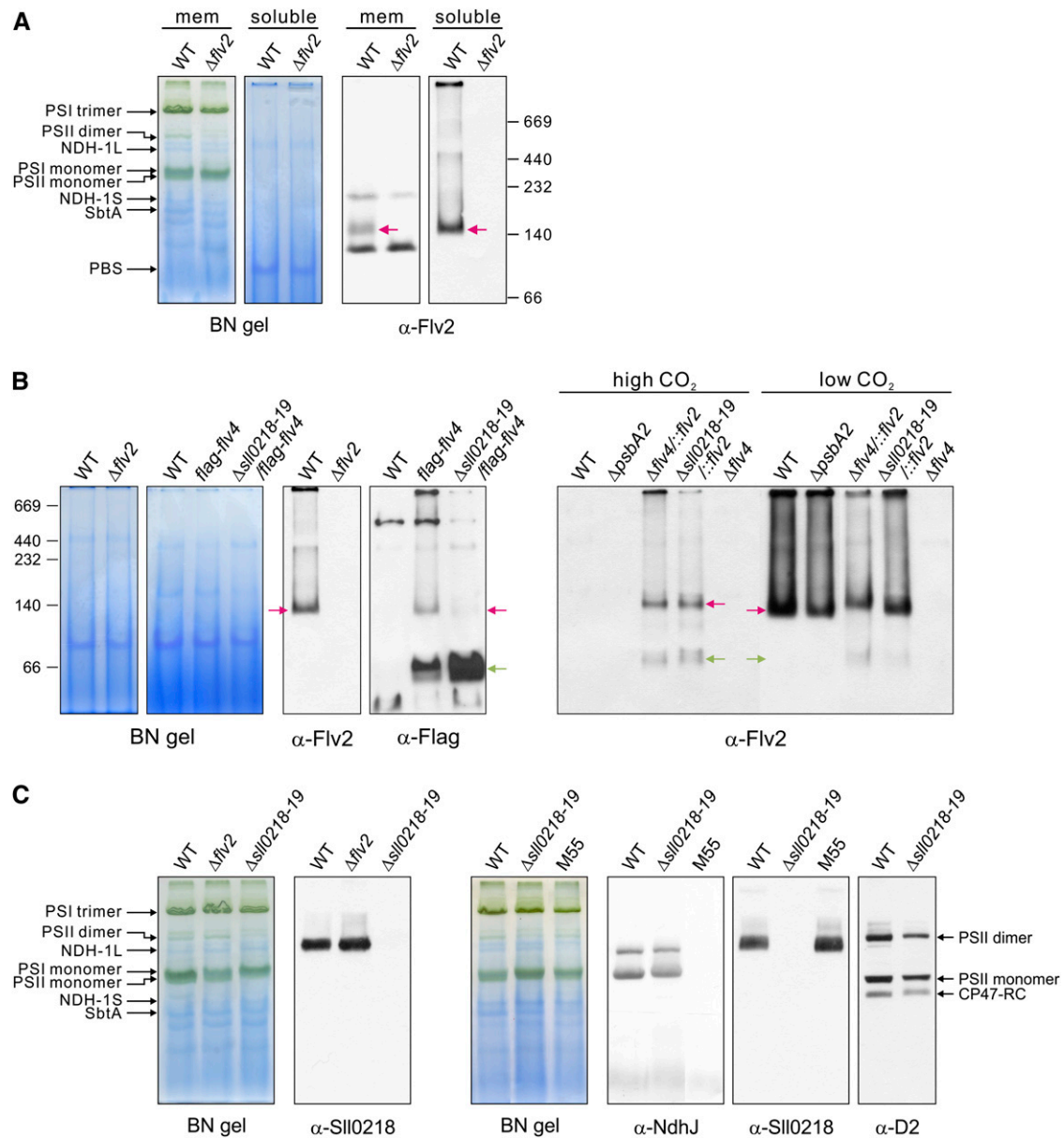


Figure 4. Protein Complexes of the Flv2, Flv4, and SII0218 Proteins in the Membrane and Soluble Fractions.

Cells were grown at air level of CO₂ (low CO₂) if not otherwise specified. Membrane (mem) and soluble fractions were isolated from wild-type (WT) and the *flv* mutant cells and separated by BN-PAGE of different acrylamide concentration (5 to 12% or 6 to 13%). BN gels and respective protein immunoblots demonstrating the Flv2 complex in the wild type (A). The $\Delta flv2$ mutant is shown as a control. The Flv2/Flv4 heterodimer in the wild type, the *flag-flv4* strains, and $\Delta psbA2$ as well as Flv2 homodimer and monomer in $\Delta flv4::flv2$ and $\Delta sII0218-19::flv2$ (B). Association of the SII0218 protein in a large membrane protein complex and demonstration of this complex not being the NDH-1 complex (α -NdhJ) (C). The red arrows demonstrate the positions of the dimeric Flv2 and Flv4 complexes, and the green arrow demonstrates the position of monomeric FLAG-Flv4. See Figure 3A for detailed description of the *flv* inactivation mutants. NdhB subunit is deleted in the M55 mutant (Ogawa, 1991), which is unable to assemble NDH-1L and NDH-1M complexes (Zhang et al., 2004).

subjected to BN/SDS-PAGE analysis (Figure 5). After BN-PAGE, three major different forms of the PSII complexes were detected: the dimer, the monomer, and the CP47-RC monomer. To quantify the amounts of the different forms of the PSII complexes, the PSII core proteins D1 and D2 were quantified by immunoblotting the

2D BN/SDS gels. The wild type had almost equal amounts of the PSII dimer and monomer, which together consisted of >80% of the total PSII complexes. All the *flv* mutants had lower amounts of PSII than the wild type. The total PSII content in $\Delta flv2$ was ~70% of that in the wild type, but the proportions of different PSII

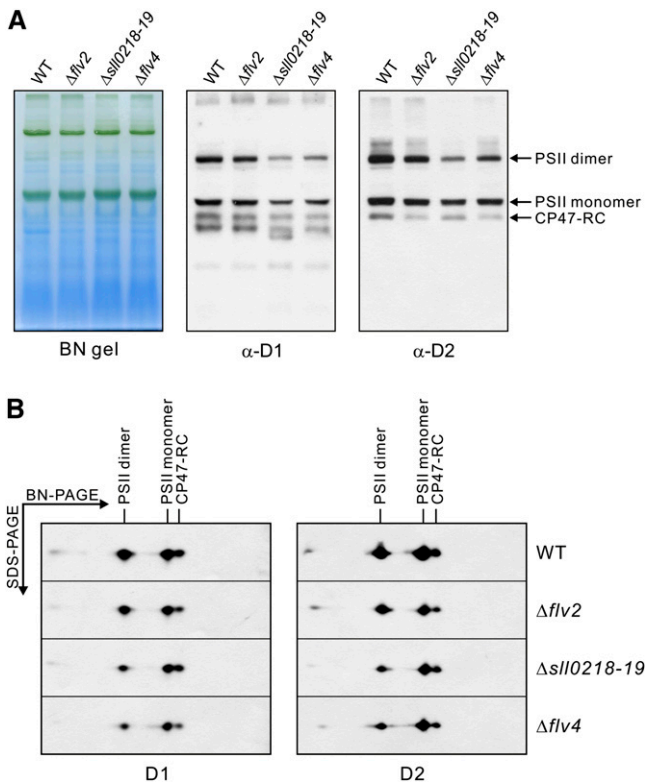


Figure 5. Different Forms of PSII Complexes in the Wild Type and the *flv* Mutants.

Membrane samples were isolated from the cells grown at air level of CO_2 and were applied to BN/SDS-PAGE. After electrotransfer, the polyvinylidene fluoride membranes were probed with the D1 and D2 antibodies. WT, the wild type.

(A) BN gels and respective protein immunoblots demonstrating the different PSII complexes.

(B) Slices of 2D BN/SDS gel immunoblots.

complexes were similar to that in the wild type. The PSII content in $\Delta sll0218-19$ and $\Delta flv4$ was only $\sim 50\%$ of that in the wild type. Moreover, the proportion of the PSII dimer was significantly lower, and the proportion of the monomeric PSII complexes (both monomer and CP47-RC) was higher compared with the wild type and $\Delta flv2$. The quantification of the PSII complexes in the wild type and the *flv* mutants is shown in Table 1. The absence of the Sll0218 protein significantly reduced the relative content of PSII dimers.

Energy Transfer from PBS to Photosystems in the Wild Type and the *flv* Mutants

To investigate whether the proteins encoded by the *flv4-flv2* operon affect the efficiency of energy transfer from PBS to the photosystems, the 77K fluorescence emission spectra were recorded from the cells grown under high or air level of CO_2 (Figure 6). When chlorophyll *a* was preferentially excited using 440-nm light, the fluorescence emission spectra showed two main peaks characteristic to PSII (685 and 695 nm) and PSI (723

nm), and differences between the wild type and all the *flv* mutants were only marginal in the cells grown both at high CO_2 and in the air (Figures 6A and 6B). When 580-nm light was used to preferentially excite PBS, three fluorescence emission maxima were recorded (Figures 6C and 6D). They originate from PBS (650 and 665 nm), PSII (685 and 695 nm), and PSI (723 nm) emission, respectively. When the spectra were normalized to PSI fluorescence, the emission from PBS was similar in the wild type and all the *flv* mutants; however, the apparent PSII fluorescence emission (685 and 695 nm) was greatly enhanced from all the *flv4-flv2* operon mutants when compared with that of the wild type grown at air level of CO_2 (Figure 6C). Such a difference between the wild type and the *flv* mutants disappeared when using high- CO_2 -grown cells (Figure 6D). The *flag-flv4* strain behaved similarly to the wild type (data not shown).

The 77K fluorescence peak from PSII contains two subpeaks at 685 and 695 nm. The peak at 695 nm is assigned to emission from the internal antenna chlorophylls in CP47. The emission at 685 nm contains contributions from both the core antenna chlorophylls in CP43 and from the allophycocyanin emitters (Vernotte et al., 1992; Karapetyan, 2008). Due to the contribution of the terminal phycobilin emitters to the PSII fluorescence maximum at 685 nm, the spectra were deconvoluted, and the fluorescence yields were calculated (see Supplemental Figure 5 and Supplemental Table 1 online). As shown in Supplemental Table 1, the F_{PBS}/F_{PSI} ratio of the fluorescence yields was not significantly different between the wild type and any of the *flv* mutant strains. On the contrary, the 695-nm emission peak did not increase proportionally with the 685-nm peak in the *flv* mutants. Therefore, the increase in 685-nm fluorescence peak is likely to be largely due to terminal phycobilin emitters rather than to the core CP43 antenna chlorophylls (Vernotte et al., 1992). These results implied an apparent inefficiency in energy transfer from PBS to PSII in the *flv* mutants grown under air level CO_2 conditions.

The 77K fluorescence spectra demonstrated that the *flv4-flv2* operon mutants have distorted energy transfer from the terminal PBS emitters to PSII in cells grown in ambient air, whereas at high CO_2 where the *flv4-flv2* operon is suppressed, neither the wild type nor the *flv* mutants showed any abnormalities in 77K fluorescence emission at 685 nm. Moreover, the 77K fluorescence emission spectrum of the $\Delta sll0218-19/flag-flv4$ mutant cells was similar to that of the $\Delta sll0218-19$ mutant grown at air level of CO_2 (see Supplemental Table 1 online), supporting

Table 1. Quantification of the Different Forms of PSII Complexes in the Wild Type and the *flv* Mutants

Strain	Total PSII (%)	Different Forms of PSII (%)		
		Dimer	Monomer	CP47-RC
The wild type	100	42 \pm 3	42 \pm 4	16 \pm 2
$\Delta flv2$	73 \pm 4	41 \pm 3	43 \pm 2	16 \pm 4
$\Delta sll0218-19$	49 \pm 8	24 \pm 2	50 \pm 5	26 \pm 3
$\Delta flv4$	53 \pm 8	29 \pm 6	51 \pm 6	20 \pm 2

The quantification was performed from four independent BN/SDS-PAGE blots. The values are the mean of the D1 and D2 signals \pm SD.

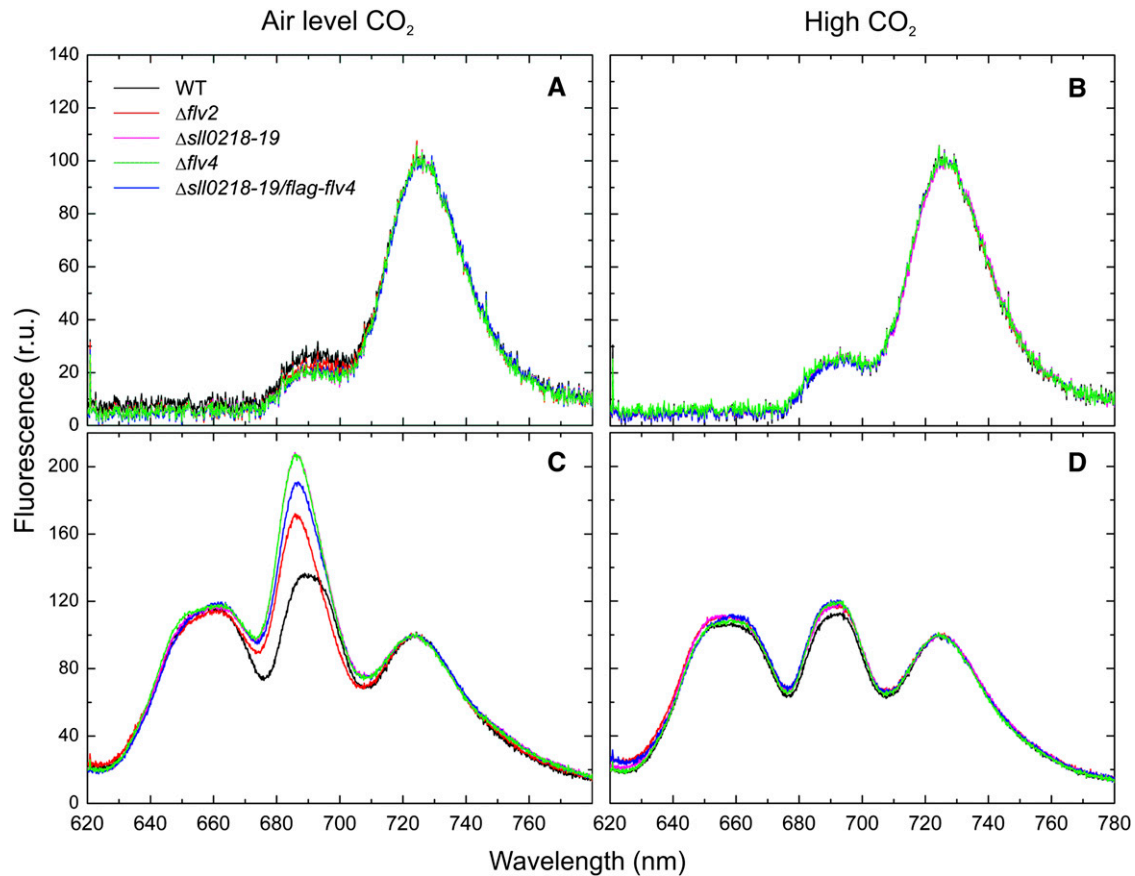


Figure 6. 77K Fluorescence Emission Spectra of the Wild Type and Various *flv* Mutant Strains.

(A) Air level of CO₂ grown cells excited by 440-nm light.

(B) High-CO₂-grown cells excited by 440-nm light.

(C) Air level of CO₂ grown cells excited by 580-nm light.

(D) High-CO₂-grown cells excited by 580-nm light.

The spectra were averaged from three to five independent measurements. Each spectrum was normalized to PSII fluorescence peak at 723 nm (set as 100), and the fluorescence was shown as relative units (r.u.). WT, the wild type.

the notion that the Flv2/Flv4 heterodimer is the functional form *in vivo*.

PSII Function in *flv4-flv2* Operon Mutants

The photosynthetic electron transfer capacity was monitored by oxygen evolution measurements using different electron acceptors (Table 2). When the cells were grown under high CO₂, there were no significant differences in the capacity of oxygen evolution between the wild type and the *flv* mutants, similar to our previous report (Zhang et al., 2009). To get further insights into the function of PSII, two different artificial electron acceptors were used; 2,6-dimethyl-*p*-benzoquinone (DMBQ), which accepts electrons from the plastoquinone (PQ) pool, and 2,6-dichloro-*p*-benzoquinone (DCBQ), which has a high affinity to the Q_B site and is suggested to accept electrons in the Q_B pocket (Graan and Ort, 1986). Generally, lower rates of oxygen evolution in the *flv* mutants than the wild type grown in the air level of CO₂ and measured in the presence of DCBQ or DMBQ

are in agreement with lower amounts of the PSII centers in the *flv* mutants (Figure 3C; Zhang et al., 2009).

The most intriguing result was a different behavior of the wild type and the *flv* mutants when DCBQ and DMBQ were used as artificial PSII electron acceptors (Table 2). The wild-type cells grown in the air level of CO₂ showed higher oxygen evolution rate with DMBQ as an artificial electron acceptor than with DCBQ. On the contrary, the oxygen evolution rates of all the *flv4-flv2* operon mutants, as well as the high-CO₂-grown wild-type cells, were higher when measured with DCBQ as an electron acceptor compared with those measured with DMBQ. Indeed, after testing several wild-type *Synechocystis* sp PCC 6803 strains of different laboratories (data not shown), all the wild-type cells grown in the air (but not the cells grown under high CO₂) showed similar behavior that strictly differs from that of all the *flv* mutants grown in the air level of CO₂ (Table 2). These results provided evidence for a presence of an additional electron exit site in wild-type cells grown in the air level of CO₂ located on, or in a close vicinity to, the Q_B site. Such electron

Table 2. Oxygen Evolution Rates of Wild-Type and *flv* Mutant Cells Measured with Different Electron Acceptors

Strain and Growth Conditions	Oxygen Evolution ($\mu\text{mol O}_2 \text{ mg}^{-1}$ Chlorophyll h^{-1})		
	Water to CO_2	Water to DCBQ	Water to DMBQ
High CO_2			
The wild type	414 \pm 27	1156 \pm 35	849 \pm 19
$\Delta flv2$	443 \pm 20	1048 \pm 11	854 \pm 10
$\Delta flv4$	411 \pm 30	1197 \pm 16	870 \pm 09
Air level of CO_2			
The wild type	437 \pm 15	547 \pm 12	663 \pm 12
$\Delta flv2$	485 \pm 18	504 \pm 11	482 \pm 17
$\Delta flv4$	444 \pm 10	508 \pm 10	457 \pm 21

Steady state oxygen evolution ($\mu\text{mol O}_2 \text{ mg}^{-1}$ chlorophyll h^{-1}) was measured by O_2 electrode under saturating light. The cells grown under high (3%) or air level of CO_2 were suspended in the growth medium. The measurements were performed in the presence of 10 mM NaHCO_3 . The results are presented as a mean \pm SD from three independent cultures and four measurements from each culture.

transfer apparently becomes inhibited by binding of DCBQ to the Q_B site, but not by the naturally functioning PQ.

The possible alternative electron transport pathway may take electrons from the Q_B site of the PSII complex and transfer them to the Flv2/Flv4 proteins. To test this hypothesis, flash-induced chlorophyll fluorescence measurements were performed (Figure 7), which reflect electron transport processes at the acceptor side of PSII. Illumination of the samples by a short saturating light pulse transfers an electron from the water-oxidizing complex of PSII to the Q_A quinone electron acceptor, which induces an increase of the fluorescence yield. Subsequent decay of fluorescence in the dark reflects the reoxidation of Q_A^- by various processes (Vass et al., 1999). Forward electron transfer to PQ, which is bound at the Q_B site at the moment of the flash, yields a 400- to 500- μs relaxation phase (fast phase). Whereas, binding of PQ to the Q_B site in centers, which did not contain Q_B at the moment of the flash, yields a 3- to 5-ms relaxation phase (middle phase). The electron that is stabilized on Q_B^- can also recombine with the S_2 state of the water-oxidizing complex via charge equilibrium between the $\text{Q}_A^- \text{Q}_B \leftrightarrow \text{Q}_A \text{Q}_B^-$ states, leading to a 10- to 15-s relaxation phase (slow phase).

Comparison of the fluorescence decay kinetics between the wild type and the $\Delta flv4$ mutant showed that in high- CO_2 -grown cells, the relaxation is practically identical in the wild type and mutant strains (Figure 7A). After shifting the cells from high CO_2 to air level of CO_2 , the overall fluorescence decay became slower in the $\Delta flv4$ mutant (Figure 7B), mainly due to the decrease of the fast phase amplitude and the higher time constant of the slow phase (Table 3). When the cells were grown in air level CO_2 , the slower fluorescence decay in the $\Delta flv4$ mutant relative to the wild type became even more clear (Table 3). These data showed that in the absence of the Flv2/Flv4 proteins, the reoxidation process of Q_A^- is slowed down. This effect provided further support for the presence of an alternative electron transfer pathway to the FDPs. However, modification of electron

transport at the acceptor side of PSII due to enhanced photo-inhibition may possibly also contribute to this behavior. The existence of an alternative electron transfer route in PSII should influence the redox state of the PQ pool by providing a pathway to keep the PQ pool oxidized. To test this hypothesis, a 2,5-dibromo-3-methyl-6-isopropyl-p-benzoquinone (DBMIB) treatment was applied, which blocks the main oxidation route of plastoquinol (PQH_2) in the PQ pool via inhibiting the Q_o site of the cytb_6/f complex. As shown in Table 3, under these conditions the fluorescence relaxation was slowed down in the high- CO_2 -grown wild type as well as the $\Delta flv4$ mutant cells, but the curves of both strains still had the same relaxation kinetics (Figure 7A). Nevertheless, after transferring the cells from high to the air level CO_2 conditions, the DBMIB effect became more pronounced in the $\Delta flv4$ mutant (Figure 7B). These data provide further evidence for the existence of an alternative electron transport pathway, which can channel out electrons from PSII and keep the PQ pool oxidized. It is worth noting that this effect was observed 48 h after the transfer of cells from high to air level of CO_2 , although the Flv2, Sl10218, and Flv4 proteins appear much

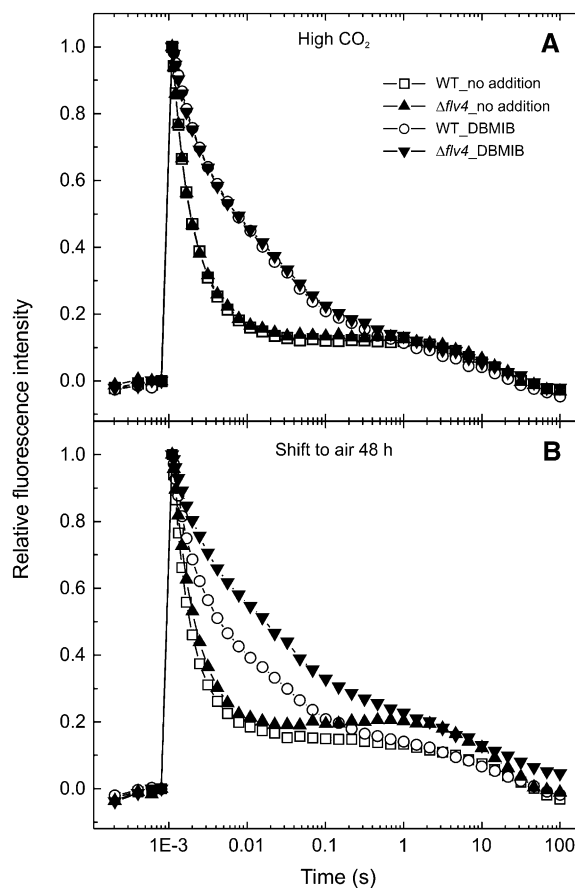


Figure 7. Relaxation of Flash-Induced Chlorophyll Fluorescence. The cells were grown under high CO_2 (A) and after a shift from high CO_2 to air for 48 h (B). The wild type, open symbols; $\Delta flv4$, closed symbols. The fluorescence traces are shown after normalization to the same initial amplitude. WT, the wild type.

Table 3. Kinetic Data of Flash-Induced Fluorescence Relaxation Components in the Wild Type and $\Delta flv4$ Mutant Grown at High CO₂, Air Level of CO₂, and 48 h after a Shift from High to Air Level of CO₂

Strains and Growth Conditions	Fast		Middle		Slow	
	T1 (ms)	A1 (%)	T2 (ms)	A2 (%)	T3 (s)	A3 (%)
High CO ₂	No addition					
The wild type	0.476 ± 0.017	58 ± 1.5	3.6 ± 0.29	26 ± 1.6	17.7 ± 1.2	16 ± 0.3
$\Delta flv4$	0.469 ± 0.007	59 ± 1.7	3.7 ± 0.15	24 ± 1.9	14.7 ± 1.2	17 ± 0.5
	+ DBMIB					
The wild type	1.360 ± 0.020	44 ± 1.5	33.6 ± 0.3	36 ± 1.7	4.3 ± 0.7	20 ± 0.2
$\Delta flv4$	1.310 ± 0.040	45 ± 1.8	36.5 ± 0.3	35 ± 2.3	3.6 ± 0.7	20 ± 0.5
Shift to air (48 h)	No addition					
The wild type	0.503 ± 0.010	64 ± 1.6	4.3 ± 0.1	20 ± 0.7	11.6 ± 3.7	16 ± 0.9
$\Delta flv4$	0.548 ± 0.045	49 ± 2.7	3.1 ± 0.5	30 ± 1.7	12.4 ± 2.8	21 ± 0.5
	+ DBMIB					
The wild type	1.015 ± 0.030	52 ± 0.3	30.6 ± 2.7	30 ± 0.6	4.7 ± 0.9	18 ± 0.3
$\Delta flv4$	1.430 ± 0.015	40 ± 1.3	39.8 ± 0.6	35 ± 2.1	4.0 ± 0.6	25 ± 0.9
Air (growth)	No addition					
The wild type	0.643 ± 0.025	65 ± 0.5	6.8 ± 0.4	19 ± 0.2	8.4 ± 1.1	16 ± 0.4
$\Delta flv4$	0.822 ± 0.028	48 ± 2.1	7.7 ± 0.3	25 ± 1.6	3.5 ± 0.2	27 ± 1.3
	+ DBMIB					
The wild type	1.030 ± 0.038	46 ± 1.5	32.1 ± 0.2	35 ± 1.8	2.2 ± 0.3	19 ± 0.4
$\Delta flv4$	1.384 ± 0.097	30 ± 1.8	35.2 ± 2.6	36 ± 2.1	1.3 ± 0.2	34 ± 0.8

Measurements were made in the absence and presence of the electron transfer inhibitor DBMIB that binds to the Q₀ site of the Cytb₆f complex. The fitting parameters of fluorescence relaxation curves are presented as a mean ± SE from three independent cultures and two to three measurements from each culture.

earlier, possibly indicating that only those PSII centers synthesized in the presence of the SII0218 proteins have a capability for alternative electron transfer to the Flv2/Flv4 heterodimer.

Homology Models of the Flv2/Flv4 Heterodimer

To analyze the Flv2/Flv4 heterodimer formation and to study how the protein(s) might dock to the membrane, the homology models of Flv2/Flv4 were constructed (Figure 8). *Synechocystis* Flv2 and Flv4 consist of three structural domains. The heterodimeric Flv2/Flv4 models were constructed for the β -lactamase-like and the flavodoxin domains. The β -lactamase-like domain (amino acids 28 to 270 in Flv2 and 19 to 250 in Flv4) contains the diiron site and the flavodoxin domain (amino acids 271 to 421 in Flv2 and 251 to 400 in Flv4) contains the FMN binding site. Conserved metal binding sites on the surface of the Flv2/Flv4 heterodimer model are summarized in Supplemental Table 2 online.

To investigate the structural changes of the enzyme during electron transfer, the Flv2/Flv4 dimer was modeled in two different oxidation states based on the structures of F₄₂₀H₂ oxidase from *Methanothermobacter marburgensis* (Seedorf et al., 2007) in the active reduced state with the switch loop in the closed conformation (Protein Data Bank [PDB] ID: 2OHI) and in the inactive oxidized state with the switch loop in the open conformation (PDB ID: 2OHJ). The sequence identity between *M. marburgensis* F₄₂₀H₂ oxidase and *Synechocystis* Flv2 and Flv4 is 29 and 26%, respectively. We also modeled the closed conformation of the Flv2/Flv4 heterodimer based on *Moorella thermoacetica* FprA (PDB ID: 1YCF), which has a sequence identity of 26% with Flv2 and 28% with Flv4. Since the sequence

identities are relatively low, the structure-based sequence alignment of the crystallized FDPs, *Synechocystis* Flv2, and Flv4 together with cyanobacterial sequences (see Supplemental Figure 6 online) was used to increase the reliability of modeling. Furthermore, the structures in the FDP family are known to represent very similar three-dimensional folds, despite sharing a sequence identity of 30 to 40%.

The Flv2/Flv4 heterodimer is formed by head-to-tail arrangement; therefore, the iron binding site in the Flv2 monomer faces the FMN binding site in the Flv4 monomer and vice versa (Figure 8A). Based on our analysis, the binding site that consists of the FMN binding site of the Flv2 monomer and the iron binding site of the Flv4 monomer (indicated with an arrow in Figures 8A and 8B) contains 10 conserved residues. In the FMN binding site of the Flv2 monomer, six FMN binding residues (Ser-285, Thr-290, and Thr-337 from Flv2 and Glu-99, His-164, and Trp-165 from Flv4) are conserved or substituted with similar residues in *M. thermoacetica* FprA (Thr-261, Thr-266, and Thr-313 from one monomer and Glu-83, His-148, and Trp-149 from the other monomer) (Figures 9A and 9B). In the closed form of the heterodimer, the iron binding residues of the Flv4 monomer (first iron, Asp-101, His-102, Asp-183, and His-240; second iron, His-97, Glu-99, and Asp-183) are totally conserved with those in *M. thermoacetica* FprA (first iron, Asp-85, His-86, Asp-167, and His-228; second iron, His-81, Glu-83, and Asp-167) (Figures 9A and 9B).

In almost all members of the FDP family, a conserved Trp stacks with the FMN isoalloxazine ring, but in methanogens and some cyanobacterial, it is replaced by Gly (Vicente et al., 2008a; pink in Supplemental Figure 6 online). This Trp is conserved in Flv2 (Trp-371) and *M. thermoacetica* FprA (Trp-347), but Flv4

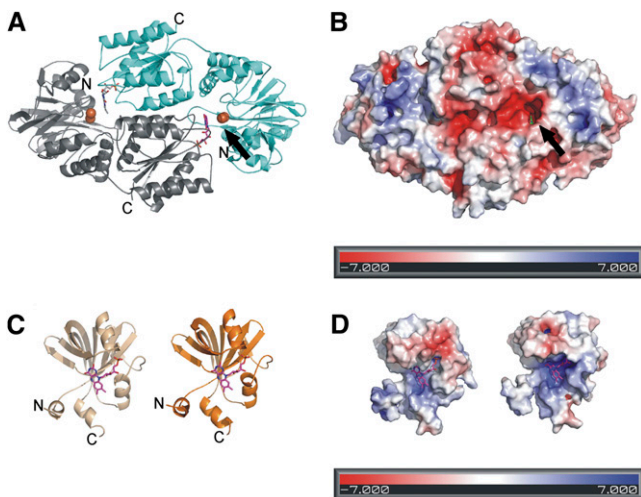


Figure 8. Homology Model of the Flv2/Flv4 Heterodimer.

- (A)** The overall fold of the Flv2/Flv4 heterodimer. The functional reactive site is seen on the right with FMN (magenta) from the Flv2 monomer (gray) and diiron site from the Flv4 monomer (cyan). The irons are shown as orange spheres.
- (B)** The electrostatic surface of the Flv2/Flv4 heterodimer. The FMN (green) is visible in the reactive site cavity.
- (C)** The homology models of the flavin reductase domains with bound FMN; Flv2 is to the left (beige) and Flv4 to the right (orange).
- (D)** The electrostatic surface of the flavin reductase domains.

and *M. marburgensis* $F_{420}H_2$ oxidase have a Gly. In the open conformation of the Flv2/Flv4 model (Figure 9D), which is based on the open conformation of *M. marburgensis* $F_{420}H_2$ oxidase (Figure 9C), Trp-371 is turned away, enlarging the binding site. Additionally, the second iron is moved and coordinated by Asp-42 and Glu-99 from Flv4 and Tyr-287 from Flv2 (Figure 9D). Furthermore, a third iron stabilizes the open conformation of the highly conserved switch loop (161-PNLH-164; Figure 9D), moving Trp-165 in Flv4 away and creating a cavity next to the FMN (Figures 9C and 9D). In the binding site formed by the FMN binding site of the Flv4 monomer and the iron binding site of the Flv2 monomer, only three residues are conserved (corresponding to His-97, Trp-165, and His-240 in Figure 9B) (see Supplemental Figure 7 online). In conclusion, the two reactive sites in the Flv2/Flv4 heterodimer differ from each other; the binding site formed by the FMN binding site of the Flv2 monomer and the iron binding site of the Flv4 monomer is more conserved than the other site and, thus, clearly functional. The FMN binding site of the Flv4 homodimer does not have all the conserved residues, whereas the iron binding sites are not conserved in the Flv2 homodimer (see Supplemental Figure 7 online). Thus, the functional binding site of the Flv2/Flv4 heterodimer structurally is even more conserved than either of the Flv homodimers.

The flavin reductase domain enables FDPs in cyanobacteria to transfer electrons directly from NAD(P)H to the catalytic iron binding site. The reaction, which in other organisms requires several steps, is condensed to a single protein (Vicente et al.,

2002). Due to unavailability of structures with all three domains, the flavin reductase domains of Flv2 and Flv4 were modeled as separate monomers (Figures 8C and 8D) based on *Archaeoglobus fulgidus* FeR (PDB ID: 110S) (Chiu et al., 2001). It has a sequence identity of 19 and 22% to Flv2 and Flv4, respectively. The *A. fulgidus* FeR dimer binds one FMN and NADP⁺. The flavin reductase domains of Flv2 and Flv4 were modeled with bound FMN, which is bound mainly by main chain interactions, supporting the previous data that many of the residues involved in binding are not conserved among FeR homologs (Chiu et al., 2001).

DISCUSSION

Synechocystis Flv4 and Flv2 Form a Functional Heterodimer in Vivo

A particular feature of cyanobacterial-type FDPs is the presence of multiple (two to six) genes encoding different FDPs in one organism. Further analyses showed that these paralogs are present in pairs, belonging to either the FlvA or the FlvB cluster (Zhang et al., 2009). Since all FDPs studied so far function as a homodimer or a homotetramer in vitro (Vicente et al., 2008b, 2009), it is conceivable that the FDPs form dimers also in cyanobacteria. In *Synechocystis*, there are two pairs of FDP genes. The *flv1* (*sl1521*) and *flv3* (*sl10550*) genes are dispersed in the genome, yet both the Flv1 and Flv3 proteins are required for the function of Mehler-like reaction (Helman et al., 2003; Allahverdiyeva et al., 2011). Here, we focused on the *flv2* (*sl10219*) and *flv4* (*sl10217*) genes, which are organized in an operon (*flv4-sl10218-flv2*), strongly induced upon low Ci and high light conditions (Zhang et al., 2009). Moreover, the gene order of the *flv4-sl10218-flv2* operon is highly conserved among cyanobacterial species (Figure 1). This also strongly suggests an interaction of the encoded proteins (Dandekar et al., 1998; Shi et al., 2005).

Interrelationship in the stability of the Flv2 and Flv4 proteins became evident from expression analysis of the *flv4-flv2* operon at both the transcript and protein levels in the wild type and various *flv* mutants. Strong downregulation of the Flv4 protein occurs in the absence of the Flv2 proteins ($\Delta flv2$ and $\Delta sl10218-19$ mutants), even though the amount of *flv4* transcripts is much higher in both mutants than in the wild type (Figure 3). Much less of the Flv2 protein was detected in the $\Delta sl10218-19::flv2$ mutant grown under high CO₂ than in the air level of CO₂ (see Supplemental Figure 4B online), despite the fact that the *psbA2* gene is expressed in an opposite manner. Such interdependency in the stability of Flv4 and Flv2 highly suggested the Flv2/Flv4 heterodimer formation. Finally, direct evidence for heterodimer formation came from a biochemical experiment with the *flag-flv4* strain (Figure 4B), which revealed the existence of the Flv2/FLAG-Flv4 heterodimer. Moreover, the Flv4 and Flv2 proteins clearly favor the heterodimer formation over the homodimer formation. Only monomeric FLAG-Flv4 was detected in $\Delta sl10218-19/flag-flv4$, indicating that the FLAG-Flv4 can hardly dimerize in vivo. Flv2, on the contrary, was found to be capable of forming homodimers in the absence of Flv4. Nevertheless, the proportion of Flv2 monomers largely decreased when Flv4 was available for

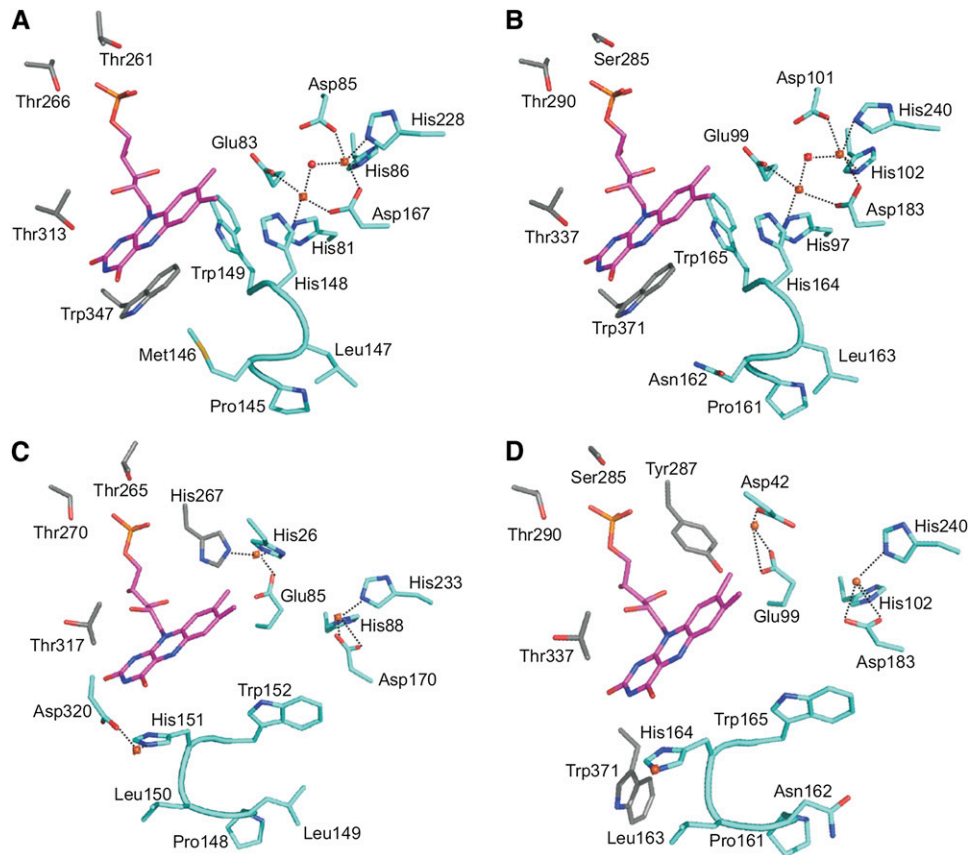


Figure 9. The FMN and Diiron Binding Sites.

- (A)** *M. thermoacetica* FprA in the closed conformation.
(B) *Synechocystis* Flv2/Flv4 heterodimer in the closed conformation
(C) *M. marburgensis* F₄₂₀H₂ oxidase in the open conformation.
(D) Flv2/Flv4 heterodimer in the open conformation.

Only the conserved active site composed of the FMN binding site of Flv2 and the diiron site of Flv4 of *Synechocystis* Flv2/Flv4 heterodimer is shown (**[B]** and **[D]**). Trp-165 of the switch loop (161-PNLH-164 in Flv4; **[B]** and **[D]**) and Trp-371 (in Flv2) turn away from the FMN, forming a cavity next to the FMN. Trp-371 is replaced by a Gly in *M. marburgensis* F₄₂₀H₂ oxidase. FMNs are shown in magenta and irons in orange. Residues participating from the other monomer are shown in gray.

heterodimer formation. Thus, we conclude that both Flv2 and Flv4 favor the Flv2/Flv4 heterodimer formation.

Molecular modeling provided further support for the Flv2/Flv4 heterodimer formation. According to the constructed homology models of the Flv2/Flv4 heterodimer, only the active site composed of the FMN binding site of Flv2 and the diiron site of Flv4 is conserved and functional, while the less-conserved active site (composed of the FMN binding site of Flv4 and diiron site of Flv2) seems not to be functional. The conserved residues from the Flv2 and Flv4 monomers together form a conserved FMN binding site in the Flv2 monomer, which in the heterodimer configuration is even more conserved than in the homodimer models (Figure 9; see Supplemental Figure 7 online). Thus, based on the analysis of the binding sites in the homology models, the Flv2/Flv4 heterodimer is capable of rapid electron transfer between FMN and the diiron center, but only one of the active sites seems to be functional.

A similar conclusion of heterodimer formation in vivo can be drawn from a functional point of view. The $\Delta sl10218-19$ mutant behaved almost similar to the $\Delta flv4$ mutant (Figures 5 and 6; Zhang et al., 2009), suggesting that the Flv4 protein is malfunctioning in the absence of Flv2. Nonfunctional Flv2 homodimer, on the other hand, can be deduced from slow kinetics of flash-induced fluorescence decay in $\Delta flv4::flv2$ cells grown under air level of CO₂ compared with $\Delta psbA2$ and $\Delta sl10218-19::flv2$ cells grown under similar conditions (see Supplemental Table 3 online).

Putative Metal Binding Sites on the Surface of the Flv2/Flv4 Heterodimer Mediate Membrane Association and Weak Protein-Protein Interactions

Strong association of the Flv2 and Flv4 proteins with the membrane fraction, despite the absence of predictable transmembrane

helices (Zhang et al., 2009), caused severe problems for characterization of the Flv4 and Flv2 proteins. It was first speculated that such a membrane association occurs via the SII0218 protein, which is an integral membrane protein with four predicted trans-membrane helices. However, this turned out not to be the case as Flv4 largely remained in the membrane fraction even in the absence of the SII0218 protein (the $\Delta flv2$, $\Delta sII0218-19$, and $\Delta sII0218-19/flag-flv4$ mutants) (data not shown). Moreover, the SII0218 protein is associated with a big membrane complex independently of the Flv2/Flv4 heterodimer (Figure 4). Finally, by modifying the two-phase partitioning method for membrane subfractionation, the SII0218 protein was localized to the thylakoid membrane, whereas Flv4 and Flv2 in that system tend to associate with the plasma membrane (Figure 2D). The latter association appeared to be strongly cation dependent (Figures 2B and 2C). Similar behavior was recently reported for another *Synechocystis* protein, although the mechanism for the membrane association is unclear (Carmel et al., 2011). Based on the Flv2/Flv4 heterodimer model and the sequence alignment, some putative metal binding sites involving His, Asp, and Glu residues were recognized on the protein surface. Surface-bound metals were found also in homologous structures. For example, the flavodoxin-like domain from *Synechococcus* sp (PDB ID: 3HLY) has a Ca^{2+} , and *M. thermoacetica* FprA (PDB ID: 1YCF, 1YCG, and 1YCH) has several Zn^{2+} bound at the surface (Silaghi-Dumitrescu et al., 2005). The metal ions on the structures originate from the crystallization solution, but some of the metal binding residues are conserved or substituted with similar residues in our model (see Supplemental Table 2 online). Taken together, these residues might be responsible for the cation-dependent association of Flv2 and Flv4 to the membrane fraction.

Based on analysis of the electrostatic surface potential of the model, the Flv4 monomer has a more negatively charged surface (Figure 8B) and contains more putative metal binding sites on the surface than the Flv2 monomer (see Supplemental Table 2 online). Taking into consideration the fact that the cation concentration used in the isolation buffer is much higher than the real physiological conditions (Figures 2B to 2D), the binding of Flv2/Flv4 to the membrane *in vivo* might be transient and reversible. Specificity of Flv2/Flv4 to plasma membrane upon cell breakage (Figure 2D) may also relate to its surface charge since the inner surface of the plasma membrane is more negative than the right-side-out thylakoid membrane (Barber, 1982; Körner et al., 1985). However, the surface charge of the thylakoid membrane can be dramatically changed during photosynthesis, which may mediate transit binding of Flv2/Flv4 also with the thylakoid membrane.

SII0218 Protein Resides in the Thylakoid Membrane and Stabilizes the PSII Dimer in Low C_i Condition

The SII0218 protein was unambiguously localized to a high molecular mass complex in the thylakoid membrane. However, the strange behavior of the SII0218 protein in the conventional two-phase partitioning system of the membrane subfractions suggested that the SII0218 protein is not evenly distributed in the thylakoid membrane. It is associated with a large complex, which is just marginally smaller than the major PSII dimer. Decrease of the ratio of PSII dimer to PSII monomer complexes

happens only in the mutants lacking the SII0218 protein ($\Delta sII0218-19$ and $\Delta flv4$), but not in $\Delta flv2$ (Figure 5, Table 1). Therefore, we postulate that the SII0218 may function as a chaperon in the stabilization of the PSII dimer assembled under conditions of air level of CO_2 .

Although the PSII complex has been isolated both in the monomeric and dimeric form (Rögner et al., 1987; Hankamer et al., 1997; Adachi et al., 2009), it is widely accepted that *in vivo* the PSII complex functions as a dimer in cyanobacteria as well as in higher plants (Hankamer et al., 1999; Kuhl et al., 2000), whereas the monomeric PSII may be an intermediate of the normal assembly and repair of PSII (Aro et al., 2005; Nixon et al., 2010). Although the *in vivo* dimerization of PSII in cyanobacteria has been questioned due to the use of detergents for solubilization and *in vitro* analysis of the thylakoid complexes (Takahashi et al., 2009; Watanabe et al., 2009), there is compelling evidence for dimer formation by mutant approaches. Indeed, small PSII subunits PsbM and PsbT, located in monomer-monomer interface, have been shown crucial for proper assembly and repair of PSII (Ohnishi and Takahashi, 2001; Iwai et al., 2004; Bentley et al., 2008). Since the SII0218 protein is expressed only under low (i.e., air level) CO_2 conditions, we postulate that the assembly of PSII dimers differs depending on the presence or absence of the SII0218 proteins (see below).

Flv2/Flv4 Heterodimer and SII0218 Protein Are Functionally Linked in Photoprotection of PSII

Optimization of photosynthesis requires strict regulation between absorption and conversion of solar energy into chemical energy and its utilization by downstream metabolic pathways. For aquatic photoautotrophs, such as cyanobacteria, CO_2 is an essential but often deficient substrate. In natural environments, insufficient availability of CO_2 , especially when combined with high irradiation, results in high excitation pressure on photosystems (Huner, 1998) and limits the rate of photosynthesis. To cope with this, several CO_2 -concentrating mechanisms are heavily induced at low C_i conditions in cyanobacteria to enhance the CO_2 concentration around ribulose-1,5-bis-phosphate carboxylase/oxygenase and at the same time induce cyclic electron flow to generate more ATP (reviewed in Kaplan and Reinhold, 1999; Giordano et al., 2005; Badger et al., 2006; Price et al., 2008). Microarray and proteomic studies have revealed a low- CO_2 stimulon (Wang et al., 2004; Eisenhut et al., 2007; Battchikova et al., 2010), also including the operon *sII0217-19* (*flv4-flv2*), which is regulated as strongly as the inducible CO_2 -concentrating mechanism genes. The *flv2* and *flv4* genes also have a high light response (Hihara et al., 2001; Zhang et al., 2009). The *flv4* and *flv2* inactivation mutants revealed a high susceptibility to photoinhibition of PSII under air level of CO_2 conditions (Zhang et al., 2009). Moreover, our recent studies on the expression of the operon revealed a tight regulation of this operon *flv4-flv2* by small regulatory RNAs (M. Eisenhut, J. Georg, S. Klähn, I. Sakurai, H. Silén, P. Zhang, W.R. Hess, and E.-M. Aro, unpublished data). Such strong induction and regulation by antisense RNAs of the *flv4-flv2* operon together with observed protection of PSII under air level of CO_2 and high light

conditions suggest a pivotal role for all three proteins under carbon-limiting conditions.

According to the results presented here, the gene products of *sll0217* and *sll0219*, the two FDPs Flv4 and Flv2, form a heterodimer and reside in the cytoplasm, although they may also occasionally be associated with the membrane *in vivo*. Low efficiency of energy transfer from PBS to PSII, most probably due to uncoupled PBS, is typical of all *flv* operon mutants (Figure 6B), suggesting that the Flv2/Flv4 heterodimer also is involved in dynamic interactions between PBS and PSII. It is important to note that this is occurring only under low ambient CO₂ conditions where the protection of PSII against photodamage by the proteins encoded by the *flv4-flv2* operon also occurs.

When energy transfer from PBS to reaction centers was studied by fluorescence spectra at 77K (Figure 6), we found a significant increase of F₆₈₅ in all *flv* inactivation mutants grown at air level of CO₂. Involvement of a chlorophyll binding protein, IsiA (Bibby et al., 2001; Boekema et al., 2001; Sandström et al., 2001), was first eliminated by showing normal fluorescence emission at 685 nm when 440-nm light was used for excitation. Similar 77K fluorescence peak at 685 nm in all the *flv* mutants and the wild type upon excitation of chlorophyll suggested that the unusual fluorescence pattern in the mutants is due to PBS. Preferential transfer of energy from PBS to PSI in the *flv* mutants was excluded since the F_{PBS}/F_{PSI} ratio is similar in the wild type and the *flv* mutants (see Supplemental Table 1 online). Involvement of nonphotochemical quenching was likewise eliminated, as it was not induced in the *flv* mutants under our standard growth conditions (data not shown). Thus, the increase of fluorescence emission at 685 nm in the *flv* mutants is concluded to result from partial uncoupling of the terminal emitters of PBS from PSII. Under normal growth conditions, the PBSs are generally associated with reaction centers and uncoupled PBSs are present in a very low amount (Mullineaux and Holzwarth, 1991). However, the *flv* mutants are exceptions and decoupled PBSs are present in low Ci growth conditions in much higher amounts than in the wild type.

Evidence has been provided indicating that PBSs are directly connected with the PSII dimer (Barber et al., 2003). However, a flexible interaction of PBS with both PSII and PSI is required for efficient energy transfer upon changes in the light regime (Mullineaux, 2008). It was suggested that PBS interacts with the thylakoid membrane via multiple weak charge-charge interactions, which allow flexible dissociation and reassociation with the reaction centers. The ApcE protein was shown to be of particular importance for the interaction of PBS with the membrane and the reaction centers (MacColl, 1998). However, the nature of the interaction between ApcE and the membrane remains obscure. We speculate, however, that the interaction between PBS and PSII, as influenced by Flv2/Flv4, is rather indirect and due to perturbation of the integrity of PSII dimers. Such perturbation also results from mutagenesis of specific subunits of PSII leading to a decrease in energy transfer efficiency from PBS to PSII (Funk et al., 1998; Veerman et al., 2005).

Although the gene products of *flv4*, *sll0218*, and *flv2* reside in different cellular locations and are associated with their own interaction partners, we assume that a functional linkage tightly connects them together. This is compatible with the conserved

gene order of the operon among a number of cyanobacterial species (Figure 1). A hypothetical model of the photoprotection mechanism by a coordinated function of the Flv2/Flv4 heterodimer and the Sll0218 protein is presented in Figure 10B. We postulate that the assembly and function of the PSII complexes require much more precise control under the deficiency of terminal electron acceptors in air level of CO₂ compared with the process under high CO₂. The Sll0218 protein is assumed to be involved in the assembly process leading to a subtle change in the conformation of the PSII dimer, which facilitates the interaction with the Flv2/Flv4 heterodimer and energy transfer between PBS and PSII. Moreover, due to a peculiar distribution of Sll0218 in the thylakoid membrane, our results provide further evidence for the presence of specific biogenesis sites of the PSII complexes (Rengstl et al., 2011).

The Flv2/Flv4 heterodimer, induced concomitantly with the Sll0218 protein, is likely to bind to the cytoplasmic side of PSII and take electrons from the Q_B site. Binding of the Flv4/Flv2 heterodimer to PSII likely occurs via charge interaction between the heterodimer and the PSII cytoplasmic side (Larom et al., 2010). The role of Flv2/Flv4 in interaction of PBS with PSII is likely to be linked to their electron transfer properties. Considering the electron transfer properties of FDPs, the fully reduced form has four-electron reduction capacity. However, our homology model of the Flv2/Flv4 heterodimer suggests that only one of the two active sites is functional. The Flv2/Flv4 heterodimer is thus likely to be capable of catalyzing a two electron transfer reaction.

One of the key observations regarding electron transport characteristics in the absence of the products of the *flv4-flv2* operon is the slower kinetic of flash-induced fluorescence decay in the $\Delta flv4$ mutant grown in the air level of CO₂ relative to the wild type, when the fluorescence curves are measured without any electron transport inhibitor (Table 3). This effect is mainly due to the increased amplitude of the middle phase of fluorescence decay, which reflects the amount of PSII centers without permanently bound PQ at the Q_B site. Occupancy of the Q_B site by PQ is determined by the amount of oxidized PQ in the pool, which is obviously decreased when higher proportion of the PQ molecules is in the fully reduced PQH₂ state. Therefore, the change of the fluorescence decay kinetic indicates an increase of PQ pool reduction in the absence of Flv2 and Flv4 proteins. A more significant manifestation of this effect is observed when PQH₂ reoxidation by the cytb₆f complex is blocked by DBMIB (Figure 7B). These data point to the existence of an alternative electron transport pathway, which involves the Flv2/Flv4 proteins and plays a significant role in the regulation of the redox level of the PQ pool. However, the possibility that modification of the Q_B binding site due to enhanced photoinhibitory damage also contributes to the change of the fluorescence decay kinetics cannot be fully excluded at this stage.

The site where the alternative pathway branches out from the electron transport route resides most likely in the PSII complex. This idea is supported by the differential effect of the DCBQ and DMBQ artificial acceptors on the electron transport and oxygen evolution rates in the wild type and the *flv* mutant strains when cultured in the air level of CO₂ (Table 2). DCBQ accepts electrons directly from the Q_B site and usually supports higher O₂

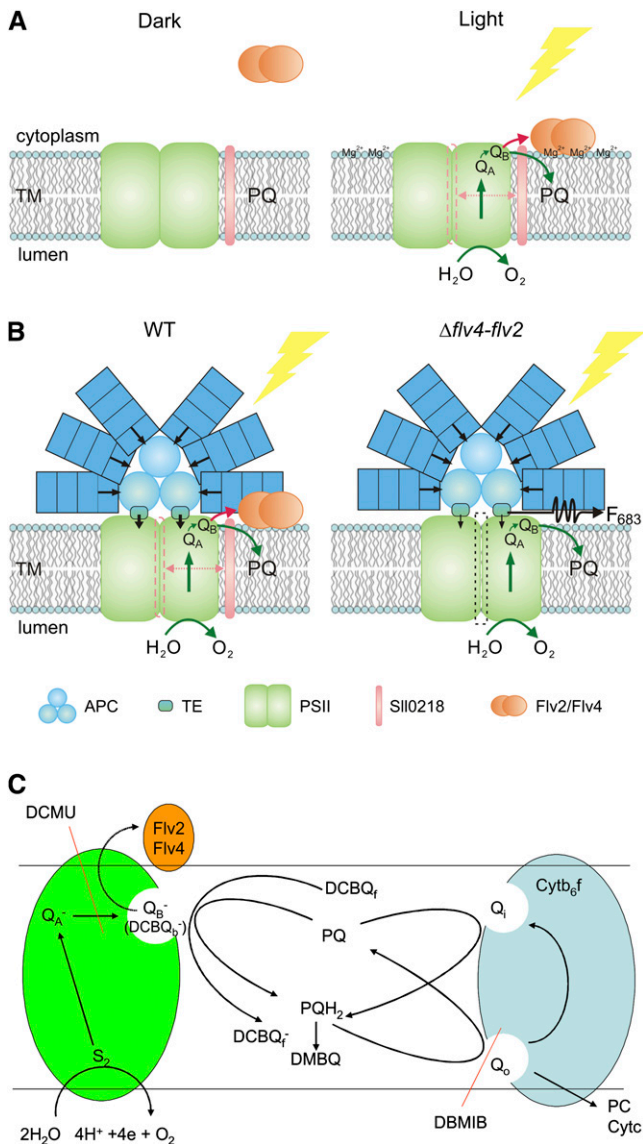


Figure 10. Working Hypothesis on the Function of the Flv2/Flv4 Heterodimer and the Sll0218 Protein during Photosynthesis at Low Ci (Air Level of CO₂) Conditions.

(A) In darkness, the Flv2/Flv4 heterodimer is mostly in soluble form in the cytoplasm. However, transient binding of the Flv2/Flv4 heterodimer to the thylakoid membrane (TM) is postulated to occur upon increase in Mg²⁺ concentration on the cytoplasmic surface of the thylakoid membrane when the lights are turned on. This creates an alternative electron transfer route from PSII to the Flv2/Flv4 heterodimer that is made possible by Sll0218-induced subtle changes in PSII.

(B) Hypothetical model for the involvement of the Flv2/Flv4 and Sll0218 proteins in energy transfer from PBS to PSII and electron transfer from PSII to the Flv2/Flv4 heterodimer at low Ci. Mg²⁺-induced attachment of the Flv2/Flv4 heterodimer to the thylakoid membrane coordinates both the energy transfer from PBS to PSII and the electron transfer from PSII to the Flv2/Flv4 heterodimer in PSII centers slightly modified by the Sll0218 protein upon the assembly process. WT, the wild type.

evolution rate than DMBQ, which takes electrons mainly from the PQ pool. This is seen here in samples that lack the Flv2/Flv4 proteins (i.e., in the mutant strains) as well as in the wild type when grown at high CO₂. However, in the wild type grown in the air, the DCBQ supported rate is smaller than the DMBQ supported rate, which indicates that occupancy of the Q_B site with DCBQ blocks the alternative electron transport pathway toward Flv2/Flv4. This idea is further supported by the kinetics of fluorescence decay (Table 3). In cells grown in the air, the PQ pool is more reduced than in the high-CO₂-grown cells due to the efficient dark reduction of PQ via the NDH-1 complex. The higher reduction level of the PQ pool leads to decreased amount of bound PQ at the Q_B site, which is also reflected in the slower decay of the flash-induced fluorescence signal. However, the observation that the fast phase is accelerated in the wild type grown in the air level of CO₂ relative to that of the $\Delta flv4$ mutant indicates that in the wild-type cells the presence of the Flv2/Flv4 proteins accelerates Q_A⁻ reoxidation. This process may take place either via electron transfer from Q_A⁻ to Flv2/Flv4 in parallel with the Q_A⁻ to Q_B process or via acceleration of Q_B⁻ reoxidation by Flv2/Flv4, which competes with the backward electron flow from Q_B⁻ to Q_A and therefore accelerates the overall reoxidation of Q_A⁻.

Based on these results, we propose the existence of an electron transport pathway from PSII to the Flv2/Flv4 proteins, which serves to decrease the high reduction level of the PQ pool under air level of CO₂ conditions. High redox level of the PQ pool results from substrate limitation and facilitates photodamage to PSII. We have a working hypothesis (Figure 10C) suggesting that the alternative electron transport pathway toward the Flv2/Flv4 proteins originates from the PSII complex, possibly from Q_B⁻. The inhibition of this process by DCBQ can arise from a structural modification of the Q_B site, which is induced by DCBQ binding. An alternative possibility is the difference in the binding affinities of Q_B⁻, which is very high and leaves sufficient time for the electron to go to the alternative route, and of DCBQ⁻, which probably has low affinity and limits the electron transfer toward Flv2/Flv4. It should be noted that analysis of the fluorescence relaxation curves is complicated by the increased level of PQ pool reduction in the Flv2/Flv4 mutants, which leads to similar changes in the fluorescence kinetics that are expected from the lack of the alternative electron transfer pathway. Therefore, the possibility that the electrons are transferred directly from PQH₂ in the lipid phase of the membrane to Flv2/Flv4 cannot be completely excluded at this stage. More precise characterization of this very interesting process, including the determination of exact redox potentials and pathways as well as their rates will require further investigation.

In conclusion, we suggest an electron transfer pathway from PSII in cyanobacteria grown under air level of CO₂. It involves a strong induction of the *flv4-flv2* operon under low Ci and high light conditions, whose protein products modify both the PBS-PSII interaction and the exit of electrons from PSII, which in turn

(C) Scheme of electron transport processes in the presence of the Flv2/Flv4 heterodimer and the functional mode of the artificial electron acceptors of PSII, DCBQ, and DMBQ.

decreases the excitation pressure on PSII in β -cyanobacteria. This is made possible by a subtle modification of the PSII dimer by the SII0218 protein, which then enables the electron transfer from PSII to the Flv2/Flv4 heterodimer. Compared with the electron donation to molecular oxygen via Flv1- and Flv3-mediated Mehler-like reaction, the electron acceptor of the Flv2/Flv4 heterodimer is not oxygen. Indeed, the electron transfer pathway from PSII to Flv2/Flv4 is a completely novel electron sink providing flexibility to PSII electron transfer, while the final electron acceptor from Flv2/Flv4 remains to be identified. Existence of such an electron transfer route may open up novel possibilities for using cyanobacteria for biotechnological purposes.

METHODS

Synechocystis Strains and Cell Culture Conditions

The *Synechocystis* sp PCC 6803 glucose-tolerant strain (Williams, 1988) was used as the wild type. The various *sII0217-19* inactivation mutants were generated by disruption of the operon by insertion of an antibiotic-resistant cassette into different positions (Figure 3A). Δ *sII0217-18* has a kanamycin-resistant cassette replacing the positions between 1384 and 2055 (Helman et al., 2003). The Δ *sII0218-19* (earlier called Δ *flv2*) has a hygromycin-resistant cassette replacing 188 to 1467 of the *sII0219* gene (Helman et al., 2003). We verified by PCR that the deletion region also partially covers the *sII0218* gene. Therefore, we renamed it as Δ *sII0218-19*. The Δ *flv4* mutant (inactivation of the entire *flv4-flv2* operon) was generated by insertion of a kanamycin-resistant cassette into 129 to 1529 of the *sII0217* gene. A new Δ *flv2* mutant was generated by insertion of a spectinomycin-resistant cassette into 403 to 1585 of the *sII0219* gene. Segregation of the *flv* inactivation mutants was verified by PCR. The *flag-flv4* and Δ *sII0218-19/flag-flv4* strains were generated by transforming the wild type and the Δ *sII0218-19* cells with self-replicating plasmid pVZ-*flag-flv4*. The plasmid was constructed by fusing the FLAG encoding sequence at the C terminus of the *flv4* gene, including the original *flv4* promoter region. The complementary strains Δ *sII0218-19::flv2* and Δ *flv4::flv2* were constructed by transformation of the *flv2* gene under *psbA2* promoter into Δ *sII0218-19* and Δ *flv4* background, respectively, and the construct was integrated into the chromosome by replacing the *psbA2* gene. Δ *psbA2* was served as a control strain for these complementary strains.

The wild-type and mutant strains were grown in BG-11 Na_2CO_3 -free medium buffered with 20 mM HEPES-NaOH, pH 7.5, except for M55 (Ogawa, 1991), which was grown in the same medium buffered with 10 mM TES-KOH, pH 8.3. The cells were illuminated under continuous photon flux density of $50 \mu\text{mol photons m}^{-2} \text{ s}^{-1}$, at 30°C . The cultures were aerated by shaking at 120 rpm at air level of CO_2 (0.038% CO_2 in the air, low CO_2). In specific cases, air enriched with 3% CO_2 (high CO_2) was applied. The mutant strains were grown in the presence of the proper antibiotics.

RNA Isolation and Real-Time Quantitative RT-PCR Analysis

Total RNA was isolated by Trizol method according to McGinn et al. (2003). After removal of genomic DNA, the first-strand cDNA was synthesized as described before (Zhang et al., 2007). The primers for analyzing the transcripts of the *flv4* and *flv2* genes, as well as the reference gene *mfpB* were the same as in (Zhang et al., 2009). The primers 5'-CTCTCAACCAATGTGGATTCG-3' and 5'-CCAGACTGACGAATTTGATGG-3' were used to analyze the *sII0218* transcripts. The primers were designed for generating a similar length (~400 bp) of amplicons. The real-

time quantitative RT-PCR was performed on a Bio-Rad IQ5 system. The annealing temperature was optimized, and the efficiency of each reaction was calculated as described earlier (Sicora et al., 2006). Gene expression of each sample was normalized to the expression level of *mfpB*. The melting curve analysis was performed to ensure the specificity of the products.

Isolation of the Membrane and Soluble Cell Fractions

The membrane and soluble fractions of *Synechocystis* cells, if not further specified, were routinely isolated as described earlier (Zhang et al., 2009) with slight modifications. In brief, the cells were pelleted from batch cultures and broken with glass beads by vortexing at 4°C in buffer B (50 mM HEPES-NaOH, pH 7.5, 30 mM CaCl_2 , 800 mM sorbitol, and 1 mM ϵ -amino-*n*-caproic acid [ACA]). The cell debris and glass beads were removed by 5 min centrifugation at 3000g. The membrane and soluble fractions were separated by centrifugation at 110,000g for 30 min. The membrane pellet was resuspended in 50 mM HEPES-NaOH, pH 7.5, 600 mM Suc, 30 mM CaCl_2 , and 1 M glycinebetaine. To study the effects of cations in the isolation buffer, the cells were broken in buffer A (20 mM potassium phosphate, pH 7.8) or in buffer C (20 mM potassium phosphate, pH 7.8, and 25 mM MgCl_2). To optimize the Mg^{2+} concentration, the buffer for disrupting the cells (50 mM HEPES-NaOH, pH 7.5, 800 mM sorbitol, and 1 mM ACA) was supplemented with different amounts of MgCl_2 (0, 1, 5, and 25 mM), CaCl_2 (0, 10, and 30 mM), or NaCl (0, 5, and 50 mM). For compatibility of the solution, buffer D (50 mM HEPES-NaOH, pH 7.5, 25 mM MgCl_2 , 800 mM sorbitol, and 1 mM ACA) was applied for isolation of the membrane fraction when subjected to two-phase partitioning.

Aqueous Two-Phase Partitioning

Two-phase partitioning was performed according to Norling et al. (1998). Additionally, a rough purification of the thylakoid and plasma membranes was performed with some modifications of the original protocol. Briefly, the total membranes were isolated from low-Ci-grown wild-type cells in buffer D and resuspended in the two-phase buffer (5 mM potassium phosphate, pH 7.4, and 0.25 M Suc) in the presence of 1 mM pefabloc. A 10-g two-phase system (5.8% [w/w] Dextran T-500, 5.8% [w/w] polyethylene glycol 3350, 5 mM potassium phosphate, pH 7.4, 0.25 M Suc, and 1 mM pefabloc) was constituted by adding 3.75 g of total membranes (1.5 mg chlorophyll) to a 6.25-g polymer mixture as described (Norling et al., 1998). A 30-g repartitioning system with the same concentrations but without the sample was prepared. After gently inverting the tube 35 times at 3°C , the phases were settled by centrifugation at 1000g for 4 min. The upper phase and the lower phase of the sample tube were collected separately. A fresh lower phase solution (5.8% Dextran) was added to the upper phase sample, and a fresh upper phase solution (5.8% polyethylene glycol) was added to the lower phase sample. After three cycles of repartitioning, the final upper and lower phases were both diluted with two-phase buffer to ~30 mL and centrifuged at 125,000g for 45 min. The pellets were washed with 20 mL of the two-phase buffer, and the centrifugation was repeated. The membranes were resuspended in a small volume of 20 mM Tricine-NaOH, pH 7.5, 10 mM NaCl, 10 mM MgCl_2 , and 500 mM Suc.

Electrophoresis and Immunoblotting

Protein complexes in the membrane and soluble fractions were analyzed by BN-PAGE, which was performed as described by Herranen et al. (2004) with minor modifications. The membrane samples were washed with 50 mM BisTris, pH 7.0, 330 mM sorbitol, and 1 mM pefabloc, pelleted by centrifugation at 18,000g for 10 min, and resuspended in 25 mM BisTris, pH 7.0, 20% glycerol (w/v), 1 mM pefabloc, and 10 mM MgCl_2 to a protein

concentration 15 $\mu\text{g}/\mu\text{L}$. The protein samples were solubilized by gently adding an equal volume of 2.5% DM in the same buffer, followed by 20 min incubation on ice and a subsequent 10-min incubation at room temperature. To remove membrane-bound DNA from the samples, 0.02 units/ μL RNase-free DNase was added during solubilization. Insoluble materials were removed by centrifugation at 18,000g for 20 min. The supernatant was mixed with one-tenth volume of sample buffer containing 5% (w/v) Serva blue G, 100 mM BisTris, pH 7.0, 30% (w/v) Suc, and 500 mM ACA and loaded to the BN gel. Solubilization was not needed for the samples of soluble fraction; instead, they were diluted in 4 \times BN buffer containing 100 mM BisTris, pH 7.0, 80% (w/v) glycerol, and 4 mM pefabloc and were ready to apply to BN-PAGE. BN-PAGE was performed according to Zhang et al. (2004). Gradient polyacrylamide gels from 5 to 12% or 6 to 13% were used in this study. SDS-PAGE was applied to analyze denatured samples. The protein samples were solubilized in Laemmli sample buffer (Laemmli, 1970) with 5% β -mercaptoethanol and 6 M urea at room temperature for 2 h and separated in 9 or 12.5% polyacrylamide gel containing 6 M urea. After electrophoresis, the proteins were electrotransferred to a polyvinylidene fluoride membrane and detected by protein-specific antibodies. The SII0218 polyclonal antibody was raised against amino acids 145 to 158 and 159 to 172 of *Synechocystis* SII0218 protein. The antibodies against Flv4, Flv2, NdhJ, D1, SbtA, and PHB3 were described earlier (Zhang et al., 2004, 2007, 2009; Boehm et al., 2009). The monoclonal anti-FLAG M2 peroxidase (horseradish peroxidase) was a commercial product from Sigma-Aldrich.

Membrane Digestion by Proteases

Membranes of the wild type were washed with 50 mM HEPES-NaOH, pH 7.5, 5 mM MgCl_2 , 10 mM NaCl, and 600 mM Suc and resuspended in the same buffer to final protein concentration of 2.5 $\mu\text{g}/\mu\text{L}$. Membranes (in final volume of 40 μL) were digested on ice for 30 min in the presence of either 0.4 μL trypsin solution (in 1 mM HCl) or 2 μL thermolysin (in 50 mM HEPES-NaOH, pH 7.5, 100 mM sorbitol, and 10 mM CaCl_2). The final protease concentrations were 0.06, 2.5, and 10 $\mu\text{g}/\text{mL}$ for trypsin and 0.02, 0.05, and 0.2 mg/mL for thermolysin. The treatments were terminated by adding an equal volume of Laemmli sample buffer and immediately heated at 65°C for 5 min.

Fluorescence Spectrometry

Low-temperature fluorescence emission spectra at 77K of the whole cells were measured by a USB4000-FL-450 spectrofluorometer. The cells were harvested at $\text{OD}_{750} = 0.6$ to 0.8 and resuspended in fresh BG-11 (Na_2CO_3 -free) medium at a chlorophyll concentration of 5 $\mu\text{g}/\text{mL}$. The resuspended cultures were acclimated under the same growth conditions for 1 h. The cells were then frozen in liquid nitrogen directly from the growth light. The cells were excited by 580 or 440 nm light obtained via 10-nm-wide filters. The fluorescence spectra were analyzed with Gaussian deconvolution, and the areas of all fluorescence sub-bands were calculated.

Flash-induced fluorescence increase and the subsequent decay of chlorophyll fluorescence yield were measured using a fluorometer FL 3500 (PSI Instruments) according to Vass et al. (1999). The cells were resuspended in fresh BG-11 medium with chlorophyll concentration 5 $\mu\text{g}/\text{mL}$ and excited with a single, short saturation flash. A fitting function with three components $[F(t) - F_0 = A1 \times \exp(-t/T1) + A2 \times \exp(-t/T2) + A3/(1 + t/T3)]$ was used for deconvolution of the measured curves according to Cser et al. (2008). $F(t)$ is the variable fluorescence yield at time t , F_0 is the basic fluorescence level before the flash, $A1$ to $A3$ are the amplitudes, and $T1$ to $T3$ are the time constants. The Joliot model (Joliot and Joliot, 1964) was used to correct the nonlinear correlation between fluorescence yield

and the redox state of Q_A with a value of 0.5 for the energy transfer parameter between the PSII units.

Oxygen Evolution Measurements

Steady state oxygen evolution was measured with a Clark-type oxygen electrode (DW1; Hansatech) at 30°C under saturating light. Before measurements, the cells were collected and resuspended in fresh growth medium at a chlorophyll concentration of 4 $\mu\text{g}/\text{mL}$. The measurements were performed by exposure of 1-mL cell suspension to 1500 $\mu\text{mol photons m}^{-2} \text{ s}^{-1}$ white light. The whole-chain photosynthesis electron transfer rates (water to CO_2) were measured in the presence of 10 mM NaHCO_3 . The PSII electron transfer rates (water to quinone) were measured in the presence of an artificial electron acceptor, either 0.5 mM DCBQ or 2 mM DMBQ. These measurements were performed also in the presence of 10 mM NaHCO_3 .

Homology Modeling of Flv2/Flv4 Heterodimer

The amino acid sequences of *Synechocystis* Flv2 (SII0219) and Flv4 (SII0217) were retrieved from Cyanobase (<http://genome.kazusa.or.jp/cyanobase>). All alignments were constructed with MALIGN (Johnson and Overington, 1993) in the Bodil visualization and modeling package (Lehtonen et al., 2004). Visualization of the alignments was done by ESPript 2.2 implemented in ENDscript 1.1 (Gouet et al., 1999). The homology models were done with MODELER (Sali and Blundell, 1993). Ten models were created for each constructed homology model, and the one with the best objective function was chosen for further analysis. The models were evaluated by Procheck (Laskowski et al., 1993). Visualization of the models was done by Pymol (<http://www.pymol.org>; deLano, 2002). The crystal structures for the multiple structure-based alignment were retrieved by BLAST searches from the PDB (<http://www.rcsb.org/>) using *Synechocystis* Flv2 and Flv4 as query sequences. The cyanobacterial sequences were retrieved by BLAST from the UniProt Knowledgebase (<http://www.ebi.ac.uk/uniprot/>). The three-dimensional models for the open and closed conformation of the β -lactamase-like and flavodoxin domains of *Synechocystis* Flv2/Flv4 heterodimer and homodimers were constructed based on the alignment and the crystal structure of $F_{420}\text{H}_2$ oxidase from the methanogenic archaea *Methanothermobacter marburgensis* (closed conformation, PDB ID: 2OHI; open conformation PDB ID: 2OHJ) (Seedorf et al., 2007). A homology model of the Flv2/Flv4 heterodimer was also constructed based on *Moorella thermoacetica* FprA (PDB ID: 1YCF), which is in the closed conformation.

To model the C-terminal flavin reductase domains of Flv2 and Flv4 BLAST searches against PDB were performed, and a multiple structure-based alignment of the retrieved sequences was created. A three-dimensional model of the flavin reductase domains of *Synechocystis* Flv2/Flv4 was constructed based on the alignment and the crystal structure of *Archaeoglobus fulgidus* ferric reductase (PDB ID: 1I0S) (Chiu et al., 2001).

Phylogenetic Analysis

A rooted phylogenetic tree was constructed from alignment of selected amino acid sequences of SII0218 homologs using ClustalX2.1 (Larkin et al., 2007) and TreeView1.6.6.

Accession Numbers

Sequence data from this article can be found in The International Nucleotide Sequence Database Collaboration under the following accession numbers: Flv4, NP_440050.1; SII0218, NP_440049.1; Flv2, NP_440048.1; and PsbA2, NP_439906.1.

Supplemental Data

The following materials are available in the online version of this article.

Supplemental Figure 1. Phylogenetic Analysis of Sll0218 in Cyanobacteria, Bacteria, and Archaea.

Supplemental Figure 2. Solubility of the Flv4, Sll0218, and Flv2 Proteins by Nonionic and Zwitterionic Detergents.

Supplemental Figure 3. BN/SDS-PAGE Demonstrating the Heterodimer Formation by Flv2 and Flv4.

Supplemental Figure 4. Expression of the FLAG-Flv4, Sll0218, and Flv2 Proteins in the Wild Type, *flv* Mutants, and the *flag-flv4* Strains.

Supplemental Figure 5. An Example of the Gaussian Sub-band Deconvolution of 77K Fluorescence Emission Spectra Excited at 580 nm in *Synechocystis* Wild-Type Cells.

Supplemental Figure 6. Multiple Structure-Based Alignment of *Methanothermobacter marburgensis* F₄₂₀H₂ Oxidase (PDB ID: 2OHI), *Synechocystis* Flv2, *Synechocystis* Flv4, *Moorella thermoacetica* FprA (PDB ID: 1YCF), *Desulfovibrio gigas* Rubredoxin Oxygen:Oxidoreductase (PDB ID: 1E5D), *Giardia intestinalis* Flavoprotein (PDB ID: 2Q9U), and *Thermotoga maritima* Flavoprotein (PDB ID: 1VME).

Supplemental Figure 7. The FMN and Diiron Binding Sites of the Flv2 and Flv4 Homodimers.

Supplemental Table 1. Ratios of Low Temperature (77K) Fluorescence Yields of PBS, PSI, and PSII (F₆₈₅ + F₆₉₅) of the Wild Type and Various *flv* Mutants Excited at 580-nm Light.

Supplemental Table 2. Conserved Metal Binding Sites on the Flv2/Flv4 Heterodimer Surface.

Supplemental Table 3. Kinetic Data of Flash-Induced Fluorescence Relaxation Components of $\Delta psbA2$ and Two *flv2* Complemented Strains Grown at High and Air Level of CO₂.

ACKNOWLEDGMENTS

We thank Wolfgang R. Hess from the University of Freiburg for kindly providing the pVZ-*flag-flv4* construct. The PsbO antibody was a kind gift from Roberto Barbato (Università del Piemonte Orientale). We also thank Mark Johnson for excellent computing facilities and for the availability of the Bio-center Finland infrastructure (bioinformatics and translational activities) at Åbo Akademi University. This work was supported by the Academy of Finland (Projects 118637 and 133299), by European Union FP7/Energy Network Projects SOLAR-H2 (contract 212508) and DirectFuel (contract 256808), by the Sigrid Juselius Foundation, Tor, Joe, and Pentti Borg Foundation, and by the National Doctoral Program in Informational and Structural Biology.

AUTHOR CONTRIBUTIONS

P.Z. performed most experiments, contributed greatly to the design of experiments, wrote the first version of the article, and made all revisions as advised by others. M.E. contributed to experiments of Sll0218 and *flag-flv4*, designed experiments, and revised the article. A.-M.B. made structural modeling of Flv2/Flv4 and wrote the corresponding part of the article. D.C. constructed $\Delta flv2$ and $\Delta flv4$ mutants and contributed to revising the article. H.M.S. constructed $\Delta psbA2$, $\Delta flv4::flv2$, and $\Delta sll0218-19::flv2$ strains and analyzed the accumulation of Flv2 and Flv4 proteins in these mutants. I.V. analyzed flash-induced fluorescence curves and constructed the model of electron transfer from PSII to Flv2/Flv4. Y.A. supervised the 77K fluorescence measurements and

contributed to revising the article. T.A.S. supervised structural modeling and contributed to revising the article. E.-M.A. was mainly responsible for experimental design and for writing of the final article.

Received December 2, 2011; revised December 2, 2011; accepted April 23, 2012; published May 8, 2012.

REFERENCES

- Adachi, H., Umena, Y., Enami, I., Henmi, T., Kamiya, N., and Shen, J.-R. (2009). Towards structural elucidation of eukaryotic photosystem II: Purification, crystallization and preliminary X-ray diffraction analysis of photosystem II from a red alga. *Biochim. Biophys. Acta* **1787**: 121–128.
- Allahverdiyeva, Y., Ermakova, M., Eisenhut, M., Zhang, P., Richaud, P., Hagemann, M., Cournac, L., and Aro, E.M. (2011). Interplay between flavodiiron proteins and photorespiration in *Synechocystis* sp. PCC 6803. *J. Biol. Chem.* **286**: 24007–24014.
- Allen, J.F. (1992). Protein phosphorylation in regulation of photosynthesis. *Biochim. Biophys. Acta* **1098**: 275–335.
- Aro, E.-M., Suorsa, M., Rokka, A., Allahverdiyeva, Y., Paakkarinen, V., Saleem, A., Battchikova, N., and Rintamäki, E. (2005). Dynamics of photosystem II: A proteomic approach to thylakoid protein complexes. *J. Exp. Bot.* **56**: 347–356.
- Badger, M.R., Price, G.D., Long, B.M., and Woodger, F.J. (2006). The environmental plasticity and ecological genomics of the cyanobacterial CO₂ concentrating mechanism. *J. Exp. Bot.* **57**: 249–265.
- Bailey, S., and Grossman, A. (2008). Photoprotection in cyanobacteria: Regulation of light harvesting. *Photochem. Photobiol.* **84**: 1410–1420.
- Barber, J. (1982). Influence of surface charges on thylakoid structure and function. *Annu. Rev. Plant Physiol.* **33**: 261–295.
- Barber, J., Morris, E.P., and da Fonseca, P.C.A. (2003). Interaction of the allophycocyanin core complex with photosystem II. *Photochem. Photobiol. Sci.* **2**: 536–541.
- Battchikova, N., Vainonen, J.P., Vorontsova, N., Keränen, M., Carmel, D., and Aro, E.-M. (2010). Dynamic changes in the proteome of *Synechocystis* 6803 in response to CO₂ limitation revealed by quantitative proteomics. *J. Proteome Res.* **9**: 5896–5912.
- Bentley, F.K., Luo, H., Dilbeck, P., Burnap, R.L., and Eaton-Rye, J.J. (2008). Effects of inactivating *psbM* and *psbT* on photodamage and assembly of photosystem II in *Synechocystis* sp. PCC 6803. *Biochemistry* **47**: 11637–11646.
- Bibby, T.S., Nield, J., and Barber, J. (2001). Iron deficiency induces the formation of an antenna ring around trimeric photosystem I in cyanobacteria. *Nature* **412**: 743–745.
- Boehm, M., Nield, J., Zhang, P., Aro, E.-M., Komenda, J., and Nixon, P.J. (2009). Structural and mutational analysis of band 7 proteins in the cyanobacterium *Synechocystis* sp. strain PCC 6803. *J. Bacteriol.* **191**: 6425–6435.
- Boekema, E.J., Hifney, A., Yakushevskaya, A.E., Piotrowski, M., Keegstra, W., Berry, S., Michel, K.P., Pistorius, E.K., and Kruij, J. (2001). A giant chlorophyll-protein complex induced by iron deficiency in cyanobacteria. *Nature* **412**: 745–748.
- Carmel, D., Mulo, P., Battchikova, N., and Aro, E.-M. (2011). Membrane attachment of Slr0006 in *Synechocystis* sp. PCC 6803 is determined by divalent ions. *Photosynth. Res.* **108**: 241–245.
- Chiu, H.J., Johnson, E., Schröder, I., and Rees, D.C. (2001). Crystal structures of a novel ferric reductase from the hyperthermophilic archaeon *Archaeoglobus fulgidus* and its complex with NADP⁺. *Structure* **9**: 311–319.

- Cser, K., Deák, Z., Telfer, A., Barber, J., and Vass, I.** (2008). Energetics of photosystem II charge recombination in *Acaryochloris marina* studied by thermoluminescence and flash-induced chlorophyll fluorescence measurements. *Photosynth. Res.* **98**: 131–140.
- Dandekar, T., Snel, B., Huynen, M., and Bork, P.** (1998). Conservation of gene order: A fingerprint of proteins that physically interact. *Trends Biochem. Sci.* **23**: 324–328.
- deLano, W.L.** (2002). The PyMOL Molecular Graphics System. (San Carlos, CA: DeLano Scientific).
- Di Matteo, A., Scandurra, F.M., Testa, F., Forte, E., Sarti, P., Brunori, M., and Giuffrè, A.** (2008). The O₂-scavenging flavodiiron protein in the human parasite *Giardia intestinalis*. *J. Biol. Chem.* **283**: 4061–4068.
- Eisenhut, M., von Wobeser, E.A., Jonas, L., Schubert, H., Ibelings, B.W., Bauwe, H., Matthijs, H.C.P., and Hagemann, M.** (2007). Long-term response toward inorganic carbon limitation in wild type and glycolate turnover mutants of the cyanobacterium *Synechocystis* sp. strain PCC 6803. *Plant Physiol.* **144**: 1946–1959.
- El Bissati, K., Delphin, E., Murata, N., Etienne, A.-L., and Kirilovsky, D.** (2000). Photosystem II fluorescence quenching in the cyanobacterium *Synechocystis* PCC 6803: Involvement of two different mechanisms. *Biochim. Biophys. Acta* **1457**: 229–242.
- Frazão, C. et al.** (2000). Structure of a dioxygen reduction enzyme from *Desulfovibrio gigas*. *Nat. Struct. Biol.* **7**: 1041–1045.
- Funk, C., Schröder, W.P., Salih, G., Wiklund, R., and Jansson, C.** (1998). Engineering of N-terminal threonines in the D1 protein impairs photosystem II energy transfer in *Synechocystis* 6803. *FEBS Lett.* **436**: 434–438.
- Giordano, M., Beardall, J., and Raven, J.A.** (2005). CO₂ concentrating mechanisms in algae: Mechanisms, environmental modulation, and evolution. *Annu. Rev. Plant Biol.* **56**: 99–131.
- Gouet, P., Courcelle, E., Stuart, D.I., and Métoz, F.** (1999). ESPript: Analysis of multiple sequence alignments in PostScript. *Bioinformatics* **15**: 305–308.
- Graan, T., and Ort, D.R.** (1986). Detection of oxygen-evolving photosystem II centers inactive in plastoquinone reduction. *Biochim. Biophys. Acta* **852**: 320–330.
- Hankamer, B., Morris, E.P., and Barber, J.** (1999). Revealing the structure of the oxygen-evolving core dimer of photosystem II by cryoelectron crystallography. *Nat. Struct. Biol.* **6**: 560–564.
- Hankamer, B., Nield, J., Zheleva, D., Boekema, E., Jansson, S., and Barber, J.** (1997). Isolation and biochemical characterisation of monomeric and dimeric photosystem II complexes from spinach and their relevance to the organisation of photosystem II *in vivo*. *Eur. J. Biochem.* **243**: 422–429.
- Helman, Y., Tchernov, D., Reinhold, L., Shibata, M., Ogawa, T., Schwarz, R., Ohad, I., and Kaplan, A.** (2003). Genes encoding A-type flavoproteins are essential for photoreduction of O₂ in cyanobacteria. *Curr. Biol.* **13**: 230–235.
- Herranen, M., Battchikova, N., Zhang, P., Graf, A., Sirpiö, S., Paakkarinen, V., and Aro, E.-M.** (2004). Towards functional proteomics of membrane protein complexes in *Synechocystis* sp. PCC 6803. *Plant Physiol.* **134**: 470–481.
- Hihara, Y., Kamei, A., Kanehisa, M., Kaplan, A., and Ikeuchi, M.** (2001). DNA microarray analysis of cyanobacterial gene expression during acclimation to high light. *Plant Cell* **13**: 793–806.
- Horton, P., Ruban, A.V., and Walters, R.G.** (1996). Regulation of light harvesting in green plants. *Annu. Rev. Plant Physiol. Plant Mol. Biol.* **47**: 655–684.
- Huner, N.P.A.** (1998). Energy balance and acclimation to light and cold. *Trends Plant Sci.* **3**: 224–230.
- Iwai, M., Katoh, H., Katayama, M., and Ikeuchi, M.** (2004). PSII-Tc protein plays an important role in dimerization of photosystem II. *Plant Cell Physiol.* **45**: 1809–1816.
- Johnson, M.S., and Overington, J.P.** (1993). A structural basis for sequence comparisons. An evaluation of scoring methodologies. *J. Mol. Biol.* **233**: 716–738.
- Joliot, A., and Joliot, P.** (1964). Etude cinétique de la réaction photochimique libérant l'oxygène au cours de la photosynthèse. *C. R. Acad. Sci.* **258**: 4622–4625.
- Kanervo, E., Suorsa, M., and Aro, E.-M.** (2005). Functional flexibility and acclimation of the thylakoid membrane. *Photochem. Photobiol. Sci.* **4**: 1072–1080.
- Kaplan, A., and Reinhold, L.** (1999). CO₂-concentrating mechanisms in photosynthetic microorganisms. *Annu. Rev. Plant Physiol. Plant Mol. Biol.* **50**: 539–570.
- Karapetyan, N.V.** (2008). Protective dissipation of excess absorbed energy by photosynthetic apparatus of cyanobacteria: Role of antenna terminal emitters. *Photosynth. Res.* **97**: 195–204.
- Kirilovsky, D.** (2007). Photoprotection in cyanobacteria: The orange carotenoid protein (OCP)-related non-photochemical-quenching mechanism. *Photosynth. Res.* **93**: 7–16.
- Kuhl, H., Kruij, J., Seidler, A., Krieger-Liszka, A., Bünker, M., Bald, D., Scheidig, A.J., and Rögner, M.** (2000). Towards structural determination of the water-splitting enzyme. Purification, crystallization, and preliminary crystallographic studies of photosystem II from a thermophilic cyanobacterium. *J. Biol. Chem.* **275**: 20652–20659.
- Körner, L.E., Kjellbom, P., Larsson, C., and Möller, I.M.** (1985). Surface properties of right side-out plasma membrane vesicles isolated from barley roots and leaves. *Plant Physiol.* **79**: 72–79.
- Laemmli, U.K.** (1970). Cleavage of structural proteins during the assembly of the head of bacteriophage T4. *Nature* **227**: 680–685.
- Larkin, M.A. et al.** (2007). Clustal W and Clustal X version 2.0. *Bioinformatics* **23**: 2947–2948.
- Larom, S., Salama, F., Schuster, G., and Adir, N.** (2010). Engineering of an alternative electron transfer path in photosystem II. *Proc. Natl. Acad. Sci. USA* **107**: 9650–9655.
- Laskowski, R.A., MacArthur, M.W., Moss, D.S., and Thornton, J.M.** (1993). PROCHECK: A program to check the stereochemical quality of protein structures. *J. Appl. Cryst.* **26**: 283–291.
- Lehtonen, J.V. et al.** (2004). BODIL: A molecular modeling environment for structure-function analysis and drug design. *J. Comput. Aided Mol. Des.* **18**: 401–419.
- MacColl, R.** (1998). Cyanobacterial phycobilisomes. *J. Struct. Biol.* **124**: 311–334.
- McGinn, P.J., Price, G.D., Maleszka, R., and Badger, M.R.** (2003). Inorganic carbon limitation and light control the expression of transcripts related to the CO₂-concentrating mechanism in the cyanobacterium *Synechocystis* sp. strain PCC6803. *Plant Physiol.* **132**: 218–229.
- Mullineaux, C.W.** (2008). Phycobilisome-reaction centre interaction in cyanobacteria. *Photosynth. Res.* **95**: 175–182.
- Mullineaux, C.W., and Emlyn-Jones, D.** (2005). State transitions: An example of acclimation to low-light stress. *J. Exp. Bot.* **56**: 389–393.
- Mullineaux, C.W., and Holzwarth, A.R.** (1991). Kinetics of excitation energy transfer in the cyanobacterial phycobilisome-photosystem II complex. *Biochim. Biophys. Acta* **1098**: 68–78.
- Müller, P., Li, X.-P., and Niyogi, K.K.** (2001). Non-photochemical quenching. A response to excess light energy. *Plant Physiol.* **125**: 1558–1566.
- Nixon, P.J., Michoux, F., Yu, J., Boehm, M., and Komenda, J.** (2010). Recent advances in understanding the assembly and repair of photosystem II. *Ann. Bot. (Lond.)* **106**: 1–16.
- Niyogi, K.K.** (1999). Photoprotection revisited: Genetics and molecular approaches. *Annu. Rev. Plant Physiol. Plant Mol. Biol.* **50**: 333–359.
- Norling, B., Zak, E., Andersson, B., and Pakrasi, H.** (1998). 2D-isolation of pure plasma and thylakoid membranes from the cyanobacterium *Synechocystis* sp. PCC 6803. *FEBS Lett.* **436**: 189–192.

- Ogawa, T. (1991). A gene homologous to the subunit-2 gene of NADH dehydrogenase is essential to inorganic carbon transport of *Synechocystis* PCC6803. *Proc. Natl. Acad. Sci. USA* **88**: 4275–4279.
- Ohnishi, N., and Takahashi, Y. (2001). PsbT polypeptide is required for efficient repair of photodamaged photosystem II reaction center. *J. Biol. Chem.* **276**: 33798–33804.
- Pisareva, T., Kwon, J., Oh, J., Kim, S., Ge, C., Wieslander, Å., Choi, J.S., and Norling, B. (2011). Model for membrane organization and protein sorting in the cyanobacterium *Synechocystis* sp. PCC 6803 inferred from proteomics and multivariate sequence analyses. *J. Proteome Res.* **10**: 3617–3631.
- Price, G.D., Badger, M.R., Woodger, F.J., and Long, B.M. (2008). Advances in understanding the cyanobacterial CO₂-concentrating-mechanism (CCM): Functional components, Ci transporters, diversity, genetic regulation and prospects for engineering into plants. *J. Exp. Bot.* **59**: 1441–1461.
- Rengstl, B., Oster, U., Stengel, A., and Nickelsen, J. (2011). An intermediate membrane subfraction in cyanobacteria is involved in an assembly network for photosystem II biogenesis. *J. Biol. Chem.* **286**: 21944–21951.
- Rögner, M., Dekker, J.P., Boekema, E.J., and Witt, H.T. (1987). Size, shape and mass of the oxygen-evolving photosystem II complex from the thermophilic cyanobacterium *Synechococcus* sp. *FEBS Lett.* **219**: 207–211.
- Sali, A., and Blundell, T.L. (1993). Comparative protein modelling by satisfaction of spatial restraints. *J. Mol. Biol.* **234**: 779–815.
- Sandström, S., Park, Y.I., Öquist, G., and Gustafsson, P. (2001). CP43', the *isiA* gene product, functions as an excitation energy dissipator in the cyanobacterium *Synechococcus* sp. PCC 7942. *Photochem. Photobiol.* **74**: 431–437.
- Saraiva, L.M., Vicente, J.B., and Teixeira, M. (2004). The role of the flavodiiron proteins in microbial nitric oxide detoxification. *Adv. Microb. Physiol.* **49**: 77–129.
- Seedorf, H., Hagemeier, C.H., Shima, S., Thauer, R.K., Warkentin, E., and Ermler, U. (2007). Structure of coenzyme F₄₂₀H₂ oxidase (FprA), a di-iron flavoprotein from methanogenic Archaea catalyzing the reduction of O₂ to H₂O. *FEBS J.* **274**: 1588–1599.
- Shi, T., Bibby, T.S., Jiang, L., Irwin, A.J., and Falkowski, P.G. (2005). Protein interactions limit the rate of evolution of photosynthetic genes in cyanobacteria. *Mol. Biol. Evol.* **22**: 2179–2189.
- Sicora, C.I., Appleton, S.E., Brown, C.M., Chung, J., Chandler, J., Cockshutt, A.M., Vass, I., and Campbell, D.A. (2006). Cyanobacterial *psbA* families in *Anabaena* and *Synechocystis* encode trace, constitutive and UVB-induced D1 isoforms. *Biochim. Biophys. Acta* **1757**: 47–56.
- Silaghi-Dumitrescu, R., Kurtz, D.M., Jrljungdahl, L.G., and Lanzilotta, W.N. (2005). X-ray crystal structures of *Moorella thermoacetica* FprA. Novel diiron site structure and mechanistic insights into a scavenging nitric oxide reductase. *Biochemistry* **44**: 6492–6501.
- Takahashi, T., Inoue-Kashino, N., Ozawa, S., Takahashi, Y., Kashino, Y., and Satoh, K. (2009). Photosystem II complex *in vivo* is a monomer. *J. Biol. Chem.* **284**: 15598–15606.
- Tikkanen, M., Grieco, M., and Aro, E.-M. (2011). Novel insights into plant light-harvesting complex II phosphorylation and 'state transitions'. *Trends Plant Sci.* **16**: 126–131.
- Tyystjärvi, E., and Aro, E.-M. (1996). The rate constant of photoinhibition, measured in lincomycin-treated leaves, is directly proportional to light intensity. *Proc. Natl. Acad. Sci. USA* **93**: 2213–2218.
- van Thor, J.J., Mullineaux, C.W., Matthijs, H.C.P., and Hellingwerf, K.J. (1998). Light-harvesting and state transitions in cyanobacteria. *Bot. Acta* **111**: 430–443.
- Vass, I., Kirilovsky, D., and Etienne, A.-L. (1999). UV-B radiation-induced donor- and acceptor-side modifications of photosystem II in the cyanobacterium *Synechocystis* sp. PCC 6803. *Biochemistry* **38**: 12786–12794.
- Veerman, J., Bentley, F.K., Eaton-Rye, J.J., Mullineaux, C.W., Vasil'ev, S., and Bruce, D. (2005). The PsbU subunit of photosystem II stabilizes energy transfer and primary photochemistry in the phycobilisome-photosystem II assembly of *Synechocystis* sp. PCC 6803. *Biochemistry* **44**: 16939–16948.
- Vernotte, C., Picaud, M., Kirilovsky, D., Olive, J., Ajlani, G., and Astier, C. (1992). Changes in the photosynthetic apparatus in the cyanobacterium *Synechocystis* sp. PCC 6714 following light-to-dark and dark-to-light transitions. *Photosynth. Res.* **32**: 45–57.
- Vicente, J.B., Carrondo, M.A., Teixeira, M., and Frazão, C. (2008a). Structural studies on flavodiiron proteins. *Methods Enzymol.* **437**: 3–19.
- Vicente, J.B., Gomes, C.M., Wasserfallen, A., and Teixeira, M. (2002). Module fusion in an A-type flavoprotein from the cyanobacterium *Synechocystis* condenses a multiple-component pathway in a single polypeptide chain. *Biochem. Biophys. Res. Commun.* **294**: 82–87.
- Vicente, J.B., Justino, M.C., Gonçalves, V.L., Saraiva, L.M., and Teixeira, M. (2008b). Biochemical, spectroscopic, and thermodynamic properties of flavodiiron proteins. *Methods Enzymol.* **437**: 21–45.
- Vicente, J.B., Testa, F., Mastronicola, D., Forte, E., Sarti, P., Teixeira, M., and Giuffrè, A. (2009). Redox properties of the oxygen-detoxifying flavodiiron protein from the human parasite *Giardia intestinalis*. *Arch. Biochem. Biophys.* **488**: 9–13.
- Wang, H.-L., Postier, B.L., and Burnap, R.L. (2004). Alterations in global patterns of gene expression in *Synechocystis* sp. PCC 6803 in response to inorganic carbon limitation and the inactivation of *ndhR*, a LysR family regulator. *J. Biol. Chem.* **279**: 5739–5751.
- Wasserfallen, A., Ragetti, S., Jouanneau, Y., and Leisinger, T. (1998). A family of flavoproteins in the domains Archaea and Bacteria. *Eur. J. Biochem.* **254**: 325–332.
- Watanabe, M., Iwai, M., Narikawa, R., and Ikeuchi, M. (2009). Is the photosystem II complex a monomer or a dimer? *Plant Cell Physiol.* **50**: 1674–1680.
- Williams, J.K.G. (1988). Construction of specific mutations in PSII photosynthetic reaction center by genetic engineering. *Methods Enzymol.* **167**: 766–778.
- Wollman, F.-A. (2001). State transitions reveal the dynamics and flexibility of the photosynthetic apparatus. *EMBO J.* **20**: 3623–3630.
- Zhang, P., Allahverdiyeva, Y., Eisenhut, M., and Aro, E.-M. (2009). Flavodiiron proteins in oxygenic photosynthetic organisms: photoprotection of photosystem II by Flv2 and Flv4 in *Synechocystis* sp. PCC 6803. *PLoS ONE* **4**: e5331.
- Zhang, P., Battchikova, N., Jansen, T., Appel, J., Ogawa, T., and Aro, E.-M. (2004). Expression and functional roles of the two distinct NDH-1 complexes and the carbon acquisition complex NdhD3/NdhF3/CupA/SII1735 in *Synechocystis* sp. PCC 6803. *Plant Cell* **16**: 3326–3340.
- Zhang, P., Sicora, C.I., Vorontsova, N., Allahverdiyeva, Y., Battchikova, N., Nixon, P.J., and Aro, E.-M. (2007). FtsH protease is required for induction of inorganic carbon acquisition complexes in *Synechocystis* sp. PCC 6803. *Mol. Microbiol.* **65**: 728–740.